的に進み，新薬の研究開発に対する貢献も大きくなる。さらに，遺伝的背景の異なる多数のヒトからiPS細胞を作製しバンク化することも毒性研究にとって非常に有用であり，将来的には，臨床試験に先立ち薬剤感受性の異なる複数のヒト検体を用いた予備毒性試験が可能となるであろう。

■幹細胞の創薬応用に関する内外の情勢

京都大学の山中伸弥教授が世界に先駆けてiPS細胞の作製に成功して以来，iPS細胞に関する活発な研究競争が繰り広げられている。最近では，iPS細胞の作製方法の改良やリプログラミングのメカニズムなどの基礎的研究に加えて，分化誘導研究や疾患特異的iPS細胞を用いた研究など創薬への応用を視野に入れた研究も実施されており，特に欧米でその傾向が強い。革新的な技術を実用化につなげる原動力になるのはベンチャー企業である場合が多いが，iPS細胞の創薬応用についてもベンチャー企業が重要な役割を担いつつある。

日本においては，リプロセル社が京大からiPS細胞のライセンスを受け，iPS細胞由来の心筋細胞塊の販売と受託毒性試験を開始している。海外，特に米国ではすでに複数のベンチャー企業がiPS細胞の創薬応用にフォーカスしてビジネスを開始している（表）。Cellular Dynamic International社はiPS細胞技術に基づいた薬剤スクリーニング・毒性試験を開始しており，最近，Roche社とiPS細胞を用いた毒性試験で提携した。iPerien社は疾患特異的iPS細胞を用いた創薬を目指しており，脊髄性筋萎縮症（SMA），筋萎縮性側索硬化症ALSやパーキンソン病などの神経難病患者からiPS細胞を作製し分化研究を開始している。Fate Therapeutics社は幹細胞研究者のネットワークを構築して参加企業にiPS関連技術の提供を行うビジネスを計画している。このようなベンチャー企業の活動はiPS関連の知財とも関わりその動向を注視していく必要がある。

■今後の展望

iPS細胞の創薬研究への応用に関する限り，細胞移植治療のようにiPS細胞の安全性は問題にならないので，現在作製されているiPS細胞を用いることが出来る。よって，分化誘導法の研究が進んでいる分野において，比較的小規模な化合物評価という形で早期に実用化が進むと考えられる。より広範に創薬に活用されるためには利便性など前述した課題の克服が必須であり，さらに，従来の創薬手法に対してiPS細胞を用いた場合の優位性を創薬研究者が実際に使用して実証していくことが重要である。疾患特異的iPS細胞については他の各論に譲るが，疾患の病態，異常をインビトロで再現するヒト疾患細胞モデルを作製できる点で画期的であり，創薬研究に対しても非常にインパクトが大きい。疾患iPS細胞を用いた病態メカニズムの研究から新たな創薬ターゲットが発見され，画期的な新薬につながることを期待したい。

これまで生命科学の分野で発見された画期的な知見や技術が医薬品の開発に大きく貢献してきた。モノクローナル抗体の作製技術は現在の抗体医薬の成功に結びついており，ヒトゲノム解読，トランスクリプトーム／プロテーオーム解析技術は数多くの創薬ターゲット候補をもたらした。トランスジェニックマウスやノックアウトマウスの作出技術は創薬ターゲットの検証に役立っている。iPS細胞はこれらの技術と同様に，あるいはそれ以上に創薬開発に貢献する潜在力を秘めている。出来るだけ多くの医療産業にかかわる研究者が，iPS細胞を実際に使ってその可能性を実証し，新たな創薬に結びつくことを願う。

文　献

1) Saravanan Karumbayaran, Bennett G. Novitch, Michaela Patterson, *et al.*: Stem Cells, 27, p806-811, 2009.
2) Stuart M Chambers, Christopher A Fasano, Eirini P Papapetrou, *et al.*: Nat. Biotechnol., 27, p275-280, 2009.
3) Jianhua Zhang, Gisela F. Wilson, Andrew G. Soerens, *et al.*: Circ. Res., 104, e30-e41, 2009.
4) Fumitaka Osakada, Zi-Bing Jin, Yasuhiko Hirami, *et al.*: J. Cell Sci., 122, p3169-3179, 2009.

Induction and Enhancement of Cardiac Cell Differentiation from Mouse and Human Induced Pluripotent Stem Cells with Cyclosporin-A

Masataka Fujiwara[1,2], Peishi Yan[1,3¤], Tomomi G. Otsuji[4,5], Genta Narazaki[1,6], Hideki Uosaki[1,6], Hiroyuki Fukushima[1,6], Koichiro Kuwahara[2], Masaki Harada[2], Hiroyuki Matsuda[7], Satoshi Matsuoka[7], Keisuke Okita[8], Kazutoshi Takahashi[8], Masato Nakagawa[8], Tadashi Ikeda[3], Ryuzo Sakata[3], Christine L. Mummery[9], Norio Nakatsuji[10,11], Shinya Yamanaka[8,12], Kazuwa Nakao[2], Jun K. Yamashita[1,6]*

1 Laboratory of Stem Cell Differentiation, Stem Cell Research Center, Institute for Frontier Medical Sciences, Kyoto University, Kyoto, Japan, **2** Department of Medicine and Clinical Science, Kyoto University Graduate School of Medicine, Kyoto, Japan, **3** Department of Cardiovascular Surgery, Kyoto University Graduate School of Medicine, Kyoto, Japan, **4** Stem Cell and Drug Discovery Institute, Kyoto Research Park, Kyoto, Japan, **5** Laboratory of Embryonic Stem Cell Research, Stem Cell Research Center, Institute for Frontier Medical Sciences, Kyoto University, Kyoto, Japan, **6** Department of Cell Growth and Differentiation, Center for iPS Cell Research and Application (CiRA), Kyoto University, Kyoto, Japan, **7** Department of Physiology and Biophysics, Kyoto University Graduate School of Medicine, Kyoto, Japan, **8** Department of Reprogramming Science, Center for iPS Cell Research and Application (CiRA), Kyoto University, Kyoto, Japan, **9** Department of Anatomy and Embryology, Leiden University Medical Centre, Leiden, the Netherlands, **10** Department of Development and Differentiation, Institute for Frontier Medical Sciences, Kyoto University, Kyoto, Japan, **11** Institute for Integrated Cell-Material Sciences (iCeMS), Kyoto University, Kyoto, Japan, **12** Gladstone Institute of Cardiovascular Disease, San Francisco, California, United States of America

Abstract

Induced pluripotent stem cells (iPSCs) are novel stem cells derived from adult mouse and human tissues by reprogramming. Elucidation of mechanisms and exploration of efficient methods for their differentiation to functional cardiomyocytes are essential for developing cardiac cell models and future regenerative therapies. We previously established a novel mouse embryonic stem cell (ESC) and iPSC differentiation system in which cardiovascular cells can be systematically induced from Flk1$^+$ common progenitor cells, and identified highly cardiogenic progenitors as Flk1$^+$/CXCR4$^+$/VE-cadherin$^-$ (FCV) cells. We have also reported that cyclosporin-A (CSA) drastically increases FCV progenitor and cardiomyocyte induction from mouse ESCs. Here, we combined these technologies and extended them to mouse and human iPSCs. Co-culture of purified mouse iPSC-derived Flk1$^+$ cells with OP9 stroma cells induced cardiomyocyte differentiation whilst addition of CSA to Flk1$^+$ cells dramatically increased both cardiomyocyte and FCV progenitor cell differentiation. Spontaneously beating colonies were obtained from human iPSCs by co-culture with END-2 visceral endoderm-like cells. Appearance of beating colonies from human iPSCs was increased approximately 4.3 times by addition of CSA at mesoderm stage. CSA-expanded human iPSC-derived cardiomyocytes showed various cardiac marker expressions, synchronized calcium transients, cardiomyocyte-like action potentials, pharmacological reactions, and ultra-structural features as cardiomyocytes. These results provide a technological basis to obtain functional cardiomyocytes from iPSCs.

Citation: Fujiwara M, Yan P, Otsuji TG, Narazaki G, Uosaki H, et al. (2011) Induction and Enhancement of Cardiac Cell Differentiation from Mouse and Human Induced Pluripotent Stem Cells with Cyclosporin-A. PLoS ONE 6(2): e16734. doi:10.1371/journal.pone.0016734

Editor: Felipe Prosper, Clinica Universidad de Navarra, Spain

Received November 1, 2010; **Accepted** December 24, 2010; **Published** February 22, 2011

Funding: This study was supported by grants from the Ministry of Education, Science, Sports and Culture of Japan, the Ministry of Health, Labour and Welfare, the New Energy and Industrial Development Organization (NEDO) of Japan, the Project for Realization of Regenerative Medicine. The funders had no role in study design, data collection and analysis, decision to publish, or preparation of the manuscript.

Competing Interests: The authors have declared that no competing interests exist.

* E-mail: juny@frontier.kyoto-u.ac.jp

¤ Current address: Cardiovascular Department, Dalian Municipal Central Hospital, Dalian, China

Introduction

Induced pluripotent stem cells (iPSCs) are novel pluripotent stem cells generated from adult tissues by reprogramming originally with transduction of a few defined transcription factors, such as Oct4, Sox2, Klf4, and c-myc [1], [2]. Establishment of iPSC lines from adult human tissue is facilitating development of cell transplantation-based regenerative strategies and establishment of patient-derived cells as disease models. Efficient differentiation and dissecting the differentiation mechanisms of target cells would significantly contribute to elucidate the pathophysiology of diseases and provide a platform for developing new therapeutic strategies for specific diseases through such as drug discovery [3], [4].

Cardiomyocytes are a major target of regenerative medicine. Although cardiomyocyte differentiation has been reported from various progenitor and adult cell sources (e.g. bone marrow, cardiac biopsies, adipose tissue, umbilical cord, mesenchymal cells, etc), overall, the efficiencies of functional cardiomyocyte appearance have been still variable (<1–5%) [5]. Pluripotent cells, embryonic stem cells (ESCs) and iPSCs have thus emerged as among the most promising stem cell sources for inducing

functional cardiomyocytes in vitro. Several induction and purification methods have been reported, starting with either mouse or human ESCs. These include stem cell aggregation in suspension and growth as embryoid bodies (EBs), co-culture with stroma cells, serum-free culture in differentiation medium, or hypoxic culture [6], [7], [8], [9], [10], [11]. Overall, the efficiency of cardiomycyte differentiation in human ESCs [6] should be still lower than in mouse ESCs [8], [11]. In view of the similarities between iPSCs and ESCs, most cardiomyocyte induction methods from iPSCs are based on those tried and tested in ESCs. Several groups have thus reported cardiomyocyte formation from mouse iPSCs using either EBs or stroma cell co-culture [12], [13], [14]. Recently, several reports on cardiomyocyte induction from human iPSCs appeared with based on EB formation though the efficiencies are still varied [15], [16], [17], [18], [19]. Other new methods robust in human iPSCs remain to be explored and maybe of particular value for preparation of transplantation cell sources as well as dissecting the differentiation mechanisms and drug discovery.

Previously, we developed a novel ESC differentiation system that recapitulates early cardiovascular development in vivo [8], [20], [21]. Flk1 (also known as vascular endothelial growth factor (VEGF) receptor-2) is the earliest differentiation marker for endothelial cells (ECs) and blood cells, and is a marker of lateral plate mesoderm [21], [22]. We induced $Flk1^+$ cells from ESCs, purified them by fluorescence-activated cell sorting (FACS), and re-cultured the purified cells. We succeeded in inducing the major cardiovascular cell types from the common $Flk1^+$ progenitor cells: vascular ECs, mural cells (pericytes and vascular smooth muscle cells) [20] and cardiomyocytes [8]. When purified $Flk1^+$ cells were cultured on mouse bone marrow-derived stromal cells, OP9 cells, spontaneously beating cardiomyocytes as well as ECs can be induced within 3–4 days (Flk-d3-4) even from a single cell. We, thus, demonstrated that ESC-derived $Flk1^+$ cells serve as cardiovascular progenitors [8], [20], [23], which was further supported with following several mouse and human studies [9], [24], [25], [26]. We also identified a $Flk1^+/CXCR4^+/$vascular endothelial $cadherin^-$ (FCV) population as highly cardiogenic progenitor cells among the progeny of $Flk1^+$ mesoderm cells at the single cell level [8]. That is, in an intermediate stage of ESC differentiation between $Flk1^+$ mesoderm cells and cardiomyocytes (Flk-d2), purified FCV population could efficiently give rise to cardiomyocytes from a single cell. The cardiogenic potential of FCV cells was 15–20 times higher than that of other cell populations among the $Flk1^+$ cell progeny. We further confirmed FCV cells can differentiate into cardiomyocytes in vivo through cell transplantation experiments [11]. FCV cells, which are detected just 1–2 days before the cardiomyocyte appearance, are so far the nearest upstream cardiac progenitors to cardiomyocytes. This system proved amenable to induce various cardiovascular cells systematically from ESCs, explore novel differentiation methods, and dissect the differentiation processes [23], [27], [28]. Indeed, we recently succeeded in demonstrating that an immunosuppressant, cyclosporin-A (CSA) showed a novel potent effect specifically on $Flk1^+$ mesoderm cells to induce a dramatic increase in FCV cardiac progenitor cells and cardiomyocytes with the use of this ESC differentiation system [11]. That is, when CSA was added to $Flk1^+$ cells co-cultured on OP9 cells, appearance of FCV progenitor cells and cardiomyocytes were increased by 10–20 times.

Recently, we were able to systematically induce cardiovascular cells from mouse iPSCs in a way almost identical to that using mouse ESCs [12]. Here, we combined our technologies in ESCs and iPSCs and showed that FCV cardiac progenitors and cardiomyocytes were efficiently expanded from mouse iPSCs by CSA treatment. Moreover, we extended the CSA method to human iPSCs and showed that CSA also successfully worked in human iPSC differentiation and efficiently enhanced the appearance of spontaneously beating cells. Human iPSC-derived cardiomyocytes showed expected molecular, structural and functional features of human cardiomyocytes. We, thus, succeeded in inducing and enhancing cardiac cell differentiation from both mouse and human iPSCs.

Methods

Antibodies

Monoclonal antibodies (MoAbs) for murine E-cadhein (ECCD2), murine Flk1 (AVAS12) were prepared and labeled in our laboratory as described previously [8], [21], [29]. MoAb for cardiac troponin-T (cTnT) (1:2000) was purchased from Neo-Markers (Fremont, CA). For staining human ESCs and iPSCs, another MoAb for cTnT (1:100) was from Santa Cruz Biotechnology (Santa Cruz, CA). MoAbs for murine and human α-actinin (1:800) was from Sigma (St Louis, Mo). MoAb of phycoerithrin (PE)-conjugated AVAS12 was purchased from eBioscience (San Diego, CA). MoAbs for biotinylated-CXCR4 was purchased from BD Pharmingen (San Diego, CA). Anti-HCN4 (1:200) and anti-Cav3.2 (1:200) antibodies were from Chemicon (Temecula, CA). Anti-Kir2.1 (1:200) and anti-connexin 43 (1:200) antibodies were from Alomone (Israel) and Invitrogen (Carlsbad, CA), respectively.

Reagents

Cyclosporin-A (a gift from Novartis Pharma) was dissolved in Dimethyl sulfoxide (DMSO) (Nacalai Tesque, Kyoto Japan) at 30 mg/mL. Dilution of 1–3 μg/mL were made in differentiation medium at the time of use. PKH67 fluorescent dye was purchased from Sigma (St. Louis, MO).

Mouse iPSC culture

A germline-competent mouse iPSC line, 20D-17, carrying Nanog promoter-driven GFP/IRES/puromycin resistant gene (Nanog-iPS cells), was maintained as previously described [30]. Briefly, iPSCs were maintained in Dulbecco's Modified Eagle Medium (DMEM) containing 15% FCS, non-essential amino acids, 1 mmol/L sodium pyruvate, 5.5 mmol/L 2-mercaptoethanol, 50 units/mL penicillin and 50 mg/mL streptomycin on feeder layers of mitomycin-C-treated mouse embryonic fibroblast (MEF) cells carrying stably incorporated puromycin-resistance gene. OP9 stroma cells were maintained as described [21].

Induction of mouse cardiomyocyte differentiation

Induction of $Flk1^+$ cells and sorting for $Flk1^+$ cells were performed as previously described [8], [12], [20]. Briefly, mouse iPSCs were first plated on to gelatin-coated dishes and cultured for 30 min to eliminate attached feeder cells, then, non-adherent cells were collected and induced to differentiation. Mouse iPSCs were cultured at a density of $1–2.5\times10^3$ cells/cm^2 in differentiation medium (DM)(alpha minimum essential medium (GIBCO, Grand Island, NY) supplemented with 10% fetal calf serum) on type IV collagen-coated dishes (Biocoat, Beckton Dickinson) or mitomycin C-treated confluent OP9 cell sheets (MMC-OP9) for 96–108 h. Cells were collected and selected by FACS to purify $Flk1^+$ cells. $Flk1^+$ cells were then plated on to MMC-OP9 at a density of $1–10\times10^3$ cells/cm^2 and cultured in differentiation medium to induce cardiac differentiation. CSA (1–3 μg/mL) was added to $Flk1^+$ cells on OP9 cells. Medium was replaced every 2 days.

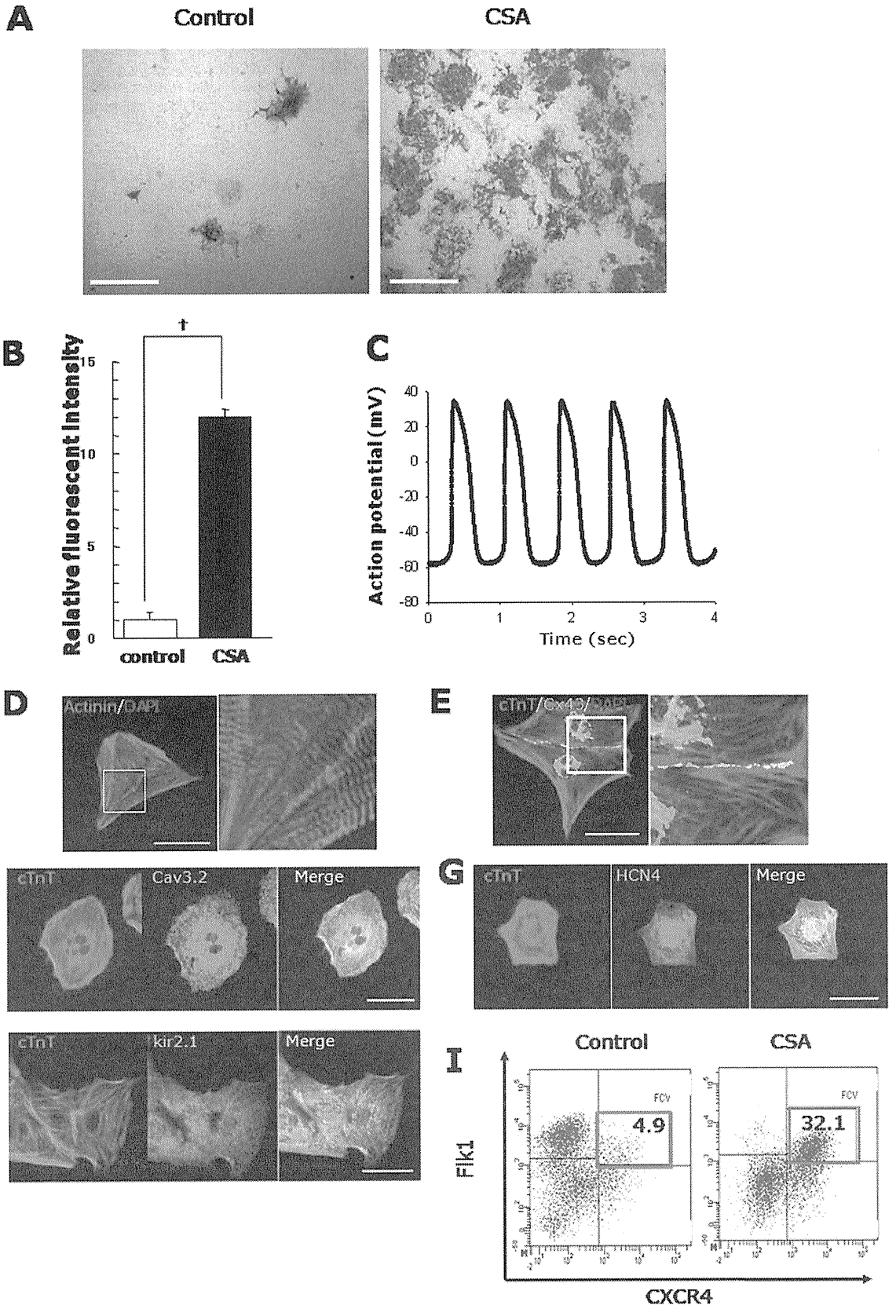

Figure 1. Cardiac cell expansion from mouse iPSC-derived Flk1$^+$ mesoderm by CSA. A. Gross appearance of cardiomyocyte induction by CSA. Six days after the Flk1$^+$ cell culture on OP9 cells (Flk-d6). cTnT staining (brown). Left panel: control. Right panel: CSA treatment. Scale bars = 400 μm. **B.** Quantitative evaluation of cardiomyocyte induction by fluorescent intensity of cTnT staining. Relative fluorescent intensity is

indicated (n = 4, †, $p<0.001$ vs control). **C.** Representative action potential of iPSC-derived spontaneously beating cardiomyocytes. **D.** Sarcomeric organization in TMRM-purified cardiomyocytes at Flk-d8. Immunostaining with anti-sarcomeric α-actinin antibody (red) and DAPI (blue). Right panel shows higher magnification of boxed area. Scale bar = 25 μm. **E–H.** Double immunostaining of TMRM-purified cardiomyocytes at Flk-d8 for connexin43 (Cx43) (green) and cTnT (orange) (E), Cav3.2 (green) and cTnT (orange) (F), HCN4 (green) and cTnT (orange) (G), Kir2.1 (green) and cTnT (orange) (H). Nuclei are visualized with DAPI. Scale bars = 25 μm. I. FACS analysis for cardiac progenitor induction from mouse iPSCs by CSA. X axis: CXCR4. Y axis: Flk1. Percentages of FCV cardiac progenitor cells (double positive population; red boxes) in total $Flk1^+$ cell progenies are indicated.
doi:10.1371/journal.pone.0016734.g001

Flowcytometry and cell sorting

FACS for differentiating mouse iPSCs was performed as described previously [8], [12], [20]. After 96–108 h of iPSC differentiation, cultured cells were harvested and stained with allophycocyanin (APC)-conjugated AVAS12 and FITC-conjugated ECCD2. Viable $Flk1^+$/E-cadherin$^-$ cells, excluding propidium iodide (Sigma), were sorted by FACS AriaII (Becton Dickinson). For FACS for FCV progenitor cells, after 2 days differentiation of purified $Flk1^+$ cell on PKH67-stained OP9 cells (Flk-d2), cultured cells were harvested and stained with a combination of MoAbs of PE-conjugated AVAS12 and biotinylated CXCR4 followed by addition of streptoavidin-conjugated APC, and subjected to FACS analysis. PKH-negative populations were analyzed and sorted as iPSC-derived cells. The $Flk1^+$/$CXCR4^+$ population (which was vascular endothelial cadherin-negative) [8] was designated "FCV cells". For FACS for cardiomyocytes, cells were harvested after 6–8 days culture of $Flk1^+$ cells on OP9 cells (Flk-d6-8). Induced cardiomyocytes were selected using tetramethyl rhodamine methyl ester (TMRM) (Invitrogen) [12], a fluorescent probe to monitor the membrane potential of mitochondria. In brief, cells were dissociated with 0.25% tryprin/EDTA, then incubated in DM with 50 nmol/L TMRM at 37°C for 15 minutes. Stained cells were washed twice and selected by FACS. TMRM-high population was considered as purified cardiomyocytes in iPSCs.

Human iPSC culture

END-2 cells were cultured as described previously [31]. Human iPS cell lines induced with transduction of four transcription factors (Oct4, Sox2, Klf4, and c-myc), 201B6 and 201B7, and Myc-negative human iPSC lines, 253G1 and 253G4 were maintained as previously described [1], [32]. 253G1 was used as the human iPS cell representative in all experiments unless stated otherwise. Induction of cardiomyocyte differentiation from human iPSCs was performed by co-culturing clumps of undifferentiated human iPSCs on END-2 cells, essentially as described previously [31]. To study the effect of CSA on cardiomyocyte differentiation, 3 μg/mL CSA was added to the culture medium on day 0 (END2-d0) or 8 (END2-d8) after start of co-culture. The number of beating colonies on END2-d12 was scored by microscopic examination. For intracellular Ca^{++} measurement and immunostaining for cTnT and actinin, beating colonies were mechanically excised, then gently dissociated by trypsin-EDTA treatment (at 37°C, 10 min), and replated on to gelatin-coated dishes. For electrophysiological analysis, beating colonies were mechanically excised and then dissociated by trypsin-EDTA with DNAse I (at 37°C, 10–15 min), and replated on to gelatin-coated dishes.

Immunohistochemistry

Immunostaining of murine cardiomyocytes was performed as described [8], [11], [12]. Briefly, 4% paraformaldehyde (PFA)-fixed cells were blocked by 2% skimmed milk (BD, bioscience) and incubated with 1st Abs. For immunohistochemistry, anti-mouse IgG –horse radish peroxidase (HRP) (Invitrogen) was used as 2nd Abs. For immunofluorescent staining, anti-mouse, rat and rabbit immunoglobulin conjugated with Alexa 488 or 546 were used for 2nd Abs. Nuclei were visualized with DAPI (Invitrogen). Cardiomyocyte differentiation was quantified as the fluorescent intensity of cTnT staining as described [8]. Immunostaining for human cardiomyocytes, 4% paraformaldehyde (PFA)-fixed cells were processed with 0.2% Triton X100 and 1% BSA (Sigma), and incubated with 1st Abs. Stained cells were photographed with inverted fluorescent microscopy, Eclipse TE2000-U (Nikon, Tokyo, Japan), digital camera system, AxioCam HRc (Carl Zeiss, Germany), or BIOREVO BZ-9000 (Keyence, Osaka, Japan).

Electrophysiology

Membrane potentials of single cells within a beating colony were measured using whole-cell patch clamp electrophysiology in the current-clamp mode (Axopatch200B, Axon Instruments/Molecular Devices Corp., Union City, CA). All recordings were carried out at room temperature [8].

Buffer compositions. Bath solution contained (in mmol/L) 140 NaCl, 5.4 KCl, 0.33 NaH_2PO_4, 0.45 $MgCl_2$, 1.8 $CaCl_2$, and 5 HEPES (pH = 7.4 with NaOH). Pipette solution contained (in mmol/L) 110 L-Aspartic acid, 30 KCl, 5 MgATP, 0.1 NaGTP, 5 K_2Creatine phosphate, 2 EGTA, 10 HEPES, and 10 NaOH (pH = 7.2 with KOH).

Field potential (FP) recordings of the beating colonies were performed using The MED64 multi-electrode array (MEA) system (Alpha MED Scientific Inc., Osaka, Japan) at a sampling rate of 20 kHz with low path filter of 500 Hz or high path filter of 1 Hz. All MEA measurements were performed at 37°C with heated perfusion system. The signals were recorded and processed with the Mobius software (WitXerx, US). The medium were perfused 1.7 ml/min as 37°C, and then the FPs were recorded for 5 min. Subsequently, E-4031(Calbiochem, US), isoproterenol (Proternol-L®, Kowa Pharmaceutical Company, Tokyo, Japan), or propranprol (Inderal®, AstraZeneca, Japan) was added to medium (discrete colony samples were used for each drug). Then, the FPs were measured for about 10 min.

Intracellular Ca measurement

Human iPSCs were loaded with 4 μM Quest Fluo-8 (ABD Bioquest, Inc. Sunnyvale, CA) for 30 min. Fluo-8 fluorescence (excitation at 495±10 nm and emission at 535±20 nm) of beating colony was measured every 16 msec with a back-thinned electron multiplier CCD camera (ImagEM; Hamamatsu Photonics, Hamamatsu, Japan). Four consecutive images were averaged. Ratio (F1/F0) to an image at minimum fluorescence intensity (F0) was calculated after background subtraction. The measurements were carried out at room temperature.

Reverse Transcription Polymerase Chain Reaction (RT-PCR)

Total RNA was isolated from various kinds of cell populations with the use of RNeasy Mini Kit (QIAGEN, Valencia, CA). cDNA was synthesized by the SuperScript III First-strand Synthesis System (Invitrogen). Polymerase chain reaction was performed with the use of KOD Plus (Toyobo, Tokyo, Japan) as described [33]. Primer sequences [34] are shown in Table S1.

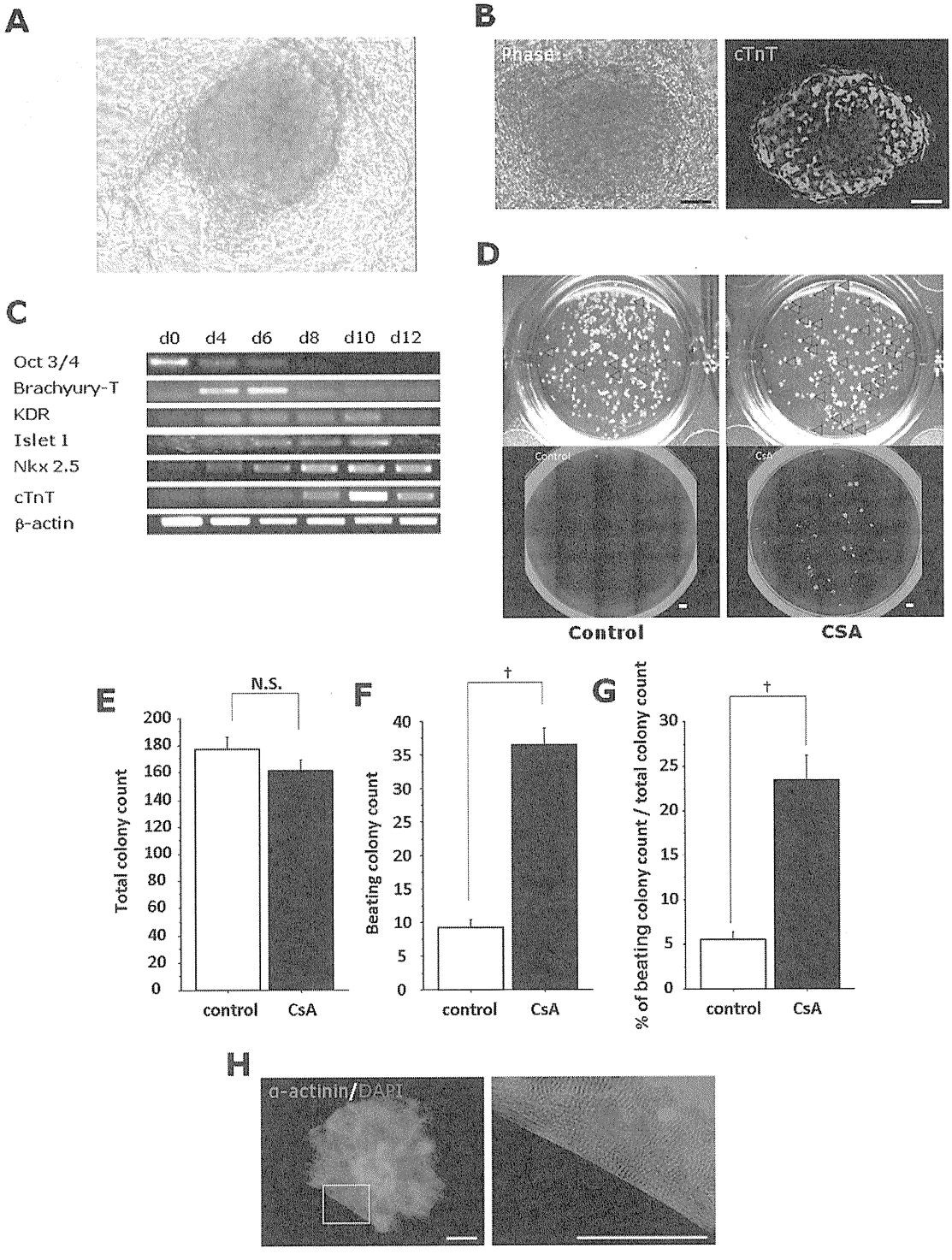

Figure 2. Induction and expansion of cardiomyocytes from human iPSCs. Human iPSCs were co-cultured with END-2 cells to differentiate cardiomyocytes. **A.** Gross morphology of a beating colony from human iPSCs (captured photo from Movie S1). **B.** cTnT staining of a beating colony on END-2 cells. Left panel: phase contrast image. Right panel: human cTnT staining (green). Scale bar = 50 μm. **C.** RT-PCR analysis for differentiation markers during cardiomyocyte differentiation of human iPSCs (from END2-d0 to d12). Oct3/4: Undifferentiated cell marker, Brachyury-T: mesendoderm marker, KDR (human Flk1): mesoderm marker, Islet1: mesoderm and cardiac progenitor marker, Nkx2.5: cardiac progenitor and cardiomyocyte marker, cTnT: cardiomyocyte marker. **D.** Representative gross appearance of human iPSC-derived beating colonies at END2-d12 in 12-well dishes. Left panels: control. Right panels: CSA treatment from END2-d8. Upper panels: phase contrast images. Beating colonies are shown by red arrows. Lower panels: cTnT staining (green). **E–G** Quantitative evaluation of beating colony appearance. **E.** Total colony count (control; 177±9.7/well (12-well dishes)(n = 8), CSA; 162±8.0/well (n = 9); N.S., p = 0.237), **F.** Beating colony count (control; 9.1±1.2/well (12-well dishes)(n = 8), CSA; 36.4±2.5/well (n = 9); †, p<0.0001), and **G.** Percentages of beating colonies (control; 5.4±0.9% (n = 8), CSA; 23.5±2.8% (n = 9); †, p<0.0001) in total colonies that appeared at END2-d12. **H.** Immunostaining of actinin (red) and DAPI (blue) in dissociated cardiomyocyte colonies. The same colony is shown in Movie S2. Right panel shows higher magnification of boxed area. Sarcomere structures are evident. Scale bar = 50 μm.
doi:10.1371/journal.pone.0016734.g002

Electron microscopic study

Human iPSC-derived beating colony was replated on multi-well chamber slide (NUNC Rochester, NewYork), fixed with 2% glutaraldehyde in 0.1 mol/L phosphate buffer (pH 7.4) for 30–60 min, washed and immersed with phosphate buffered saline for overnight at 4°C, and fixed in 1% buffered osmium tetroxide. The specimens were then dehydrated through graded ethanol and embedded in epoxy resin. Ultrathin sections (90 nm), double-stained with uranyl acetate and lead citrate, were examined under electron microscopy (H-7650; Hitachi, Tokyo, Japan).

Statistical Analysis

All data were obtained from at least three independent experiments. Statistical analysis of the data was performed using Student's t-test or ANOVA. $p<0.05$ was considered significant. All data are shown as mean ± S.D.

Results

Cardiomyocyte and cardiac progenitor expansion from mouse iPSCs by CSA

Recently, we reported that functional cardiomyocytes were induced from mouse iPSCs with our differentiation method in mouse ES cells [12]. In brief, undifferentiated mouse iPSC colonies maintained on MEFs were morphologically similar to mouse ESCs. We induced mesoderm differentiation from mouse iPSCs by culturing on type IV collagen-coated dish with DM (see Methods). $Flk1^+$ mesoderm cells that appeared were selected by FACS at 4.5 days of differentiation (iPS-d4.5) and then underwent a cardiomyocyte induction protocol involving co-culture on OP9 stroma cells; spontaneously beating cardiomyocytes began to appear after 3 to 4 days of culture (Flk-d3-4). Beating cells that appeared were positive for multiple cardiomyocyte markers and had electrophysiological features assessed by whole-cell patch clamp as previously reported [8], [12].

In the present study, we first tried to expand cardiomyocytes and cardiac progenitors from mouse iPS cells by CSA. When CSA was added to purified $Flk1^+$ cells, the appearance of $cTnT^+$ cardiomyocytes was increased 12-fold compared to controls (Fig. 1A, B), which was comparable with the increase observed in mouse ESCs [11]. CSA-expanded cardiomyocytes spontaneously beat and showed cardiomyocyte-like action potential (average interval: 0.74 sec, maximum diastolic potential: −58.6 mV and overshoot: 34.3 mV (n = 6)) (Fig. 1C). These cardiomyocytes also showed distinct sarcomere formation (Fig. 1D), expression of cTnT (Fig. 1E-H) and connexin 43 located at cellular boundaries (Fig. 1E). T-type calcium channel Cav3.2 (Fig. 1F), a pacemaker ion channel, HCN4 (Fig. 1G), and a ventricular ion channel, kir2.1 (Fig. 1H) were also detected in $cTnT^+$ cells. We also examined the effect of CSA on the induction of FCV cardiac progenitor cells in mouse iPSCs. Addition of CSA to $Flk1^+$ cells specifically increased the FCV population in mouse iPSCs to approximately 6.5 times of control. The maximum percentage of FCV cells within total $Flk1^+$ cell-derived cells was more than 30% by CSA (Fig. 1I), comparable with that observed in mouse ESCs, previously [11]. CSA can thus efficiently enhance the differentiation of functional cardiomyocytes and cardiac progenitors from mouse iPSCs.

Differentiation of cardiomyocytes from human iPSCs

We next examined cardiomyocyte differentiation from human iPSCs. We employed a human ESC differentiation method for cardiomyocytes using END-2 visceral endodermal stroma cells [31]. When human iPSCs were cultured on END-2 cells, spontaneously beating cardiomyocytes were successfully induced (Fig. 2A, Movie S1). Beating colonies were first detected after END2-d10 and became maximally evident after END2-d12.

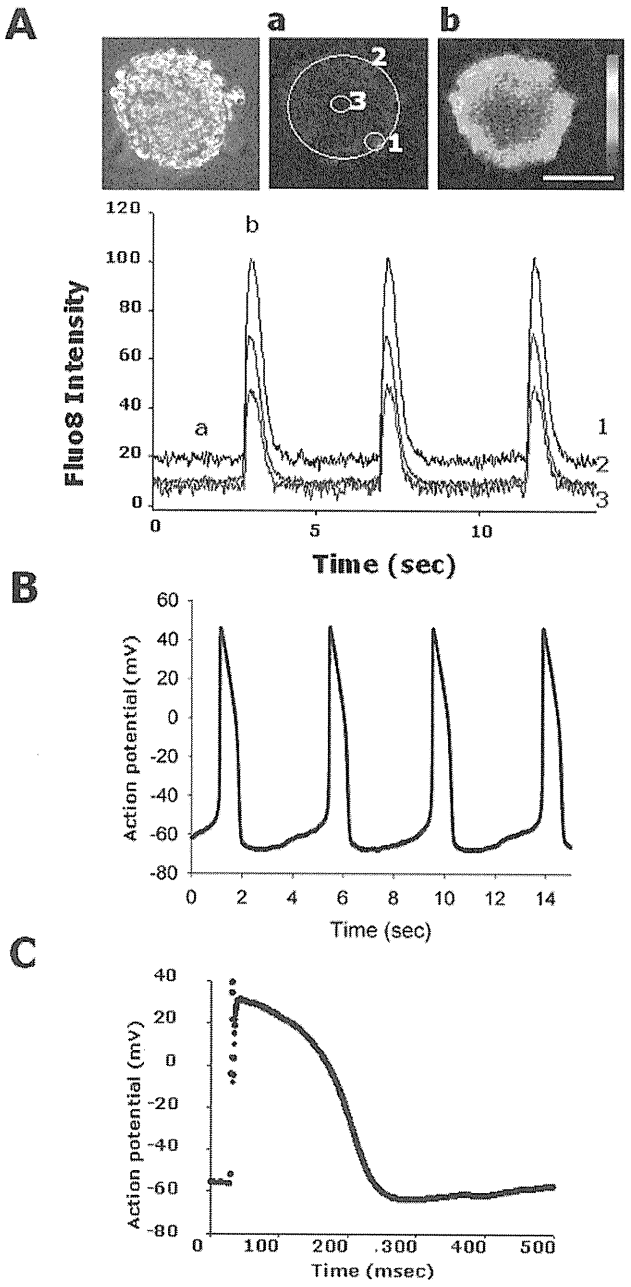

Figure 3. Functional analysis of expanded human cardiomyocytes. A. Ca^{++} transient in dissociated beating colonies. Cytoplasmic Ca^{++} change was monitored with fluo-8. Left panel: a transmission image of fluo-8 loaded iPSC colony. Middle and right panels: Fluo-8 images at the end (a) and the peak (b) of the fluorescence change. Scale bar = 50 μm. Lower panel: Time course of fluo-8 intensity change. The intensity was measured at the periphery (1), the entire colony (2) and the center (3) (ROIs shown in middle panel). Ratios (F1/F0) of the intensity to the one at the beginning of recording (F0) are indicated. Note that Ca transient is well synchronized within the colony. Real time video is shown in Movie S3. **B.** Representative action potential recorded from a cell in a beating colony. **C.** Representative single whole cell patch-cramp recording of a non-self beating human iPSC-derived cardiomyocyte after electrical stimulation.
doi:10.1371/journal.pone.0016734.g003

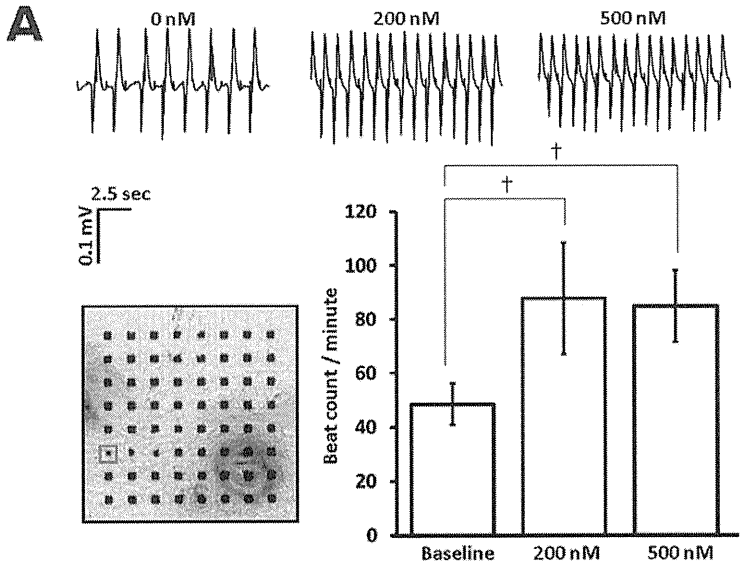
A
0 nM
200 nM
500 nM
2.5 sec
0.1 mV
Beat count / minute
120
100
80
60
40
20
0
Baseline
200 nM
500 nM
†
†

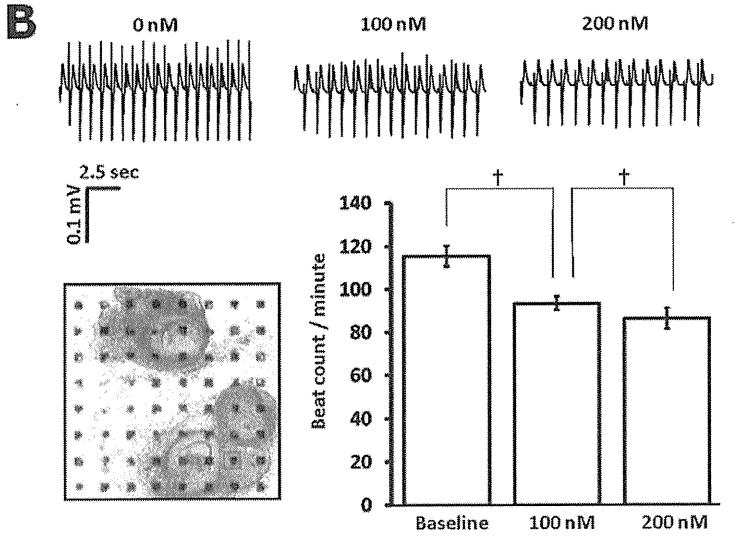
B
0 nM
100 nM
200 nM
2.5 sec
0.1 mV
Beat count / minute
140
120
100
80
60
40
20
0
Baseline
100 nM
200 nM
†
†

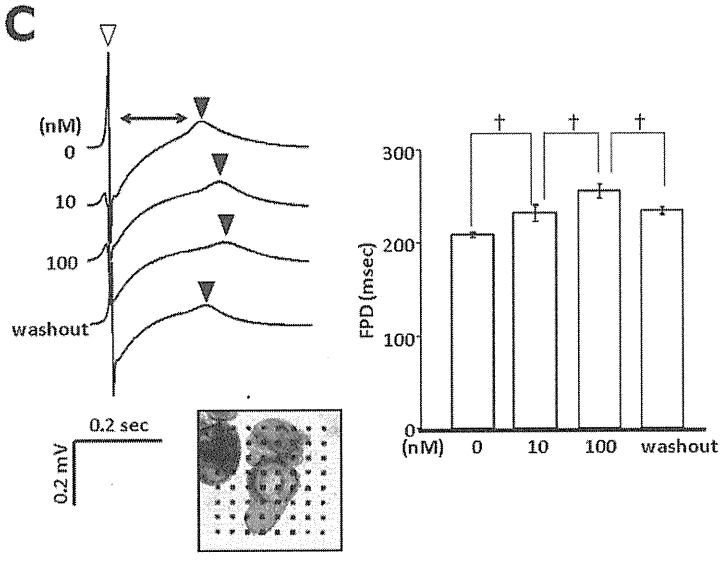
C
(nM)
0
10
100
washout
0.2 sec
0.2 mV
FPD (msec)
300
200
100
0
(nM) 0 10 100 washout
†
†
†

Figure 4. Pharmacological responses of human iPSC-derived cardiomyocytes. Field potential recordings of replated beating colonies after stimulation with isoproterenol (**A**), propranorol (**B**), and E-4031 (**C**). Photos; array of multi-electrode and replated colonies. Data recorded at electrodes in red squares are shown. **A, B.** Beating frequency (beating/minite). **C.** QT elongation. The time period from the first negative peak (open triangle) to the first positive peaks (closed triangles) reflects QT time in electrocardiogram. n = 3, †, $p<0.001$.
doi:10.1371/journal.pone.0016734.g004

These beating colonies were positive for cTnT (Fig. 2B). During the differentiation of human iPSCs on END2 cells, sequential expression of various marker genes expected for cardiomyogenesis was observed (ex: Oct3/4; undifferentiated iPSCs, Brachyury; mesendoderm, KDR; mesoderm, islet1; mesoderm and cardiac progenitors, nkx2.5; cardiac progenitors and cardiomyocytes, cTnT; cardiomyocytes) (Fig. 2C). In our another previous study on human ESC differentiation, a Flk1 (in human, VEGF receptor-2)$^{+}$/TRA1-60^{-} mesoderm population appeared in culture approximately 8 days after induction of differentiation [35]. When CSA was added to differentiating human iPSCs at the mesoderm stage (i.e. on END2-d8), the appearance of beating colonies was increased (Fig. 2D) although no effect was observed with the CSA treatment on undifferentiated human iPSCs (i.e. from END2-d0) (data not shown). Whereas the total number of iPSC-derived colonies that appeared was not changed (Fig. 2E), the number and percentage of beating colonies that appeared at END2-d12 were significantly increased approximately 4.0 and 4.3 times by CSA treatment, respectively (Fig. 2F, G). Approximately 23±2.7% of total colonies was beating in average, and in an optimized condition, 39% of total colonies included beating cardiomyocytes. CSA-expanded colonies maintained self-beating after a mechanical isolation and re-plating, and were positive for α-actinin with distinct sarcomere formation (Fig. 2H, Movie S2). Thus, cardiomyocyte induction from human iPSCs could be similarly enhanced by CSA. The mesoderm stage-specific effect of CSA in human iPSCs suggests the similar machinery in mouse ES/iPSCs are robustly working in human iPSC differentiation to cardiomyocytes.

Functional features of expanded human iPSC-derived cardiomyocytes

We next evaluated functional features of CSA-expanded human iPSC-derived cardiomyocytes. Fluo-8 imaging revealed synchronized increases in intracellular Ca^{++} in beating colonies with contraction (Fig. 3A, Movie S3). Action potentials recorded by patch clamp electrophysiology identified cells with pacemaker potential (average of the interval: 4.26 sec, maximum diastolic potential: −67.6 mV overshoot: 46.6 mV (n = 6))(Fig. 3B). Replated colonies continued beating spontaneously for more than 10 months. Some isolated single cells obtained from beating colonies at 3 months culture period lost automaticity and showed some features of human ventricular cells such as action potential with rapid depolarization and prolonged plateau after electrical stimulation (Fig. 3C). These results indicate that various functional human cardiomyocytes could be induced in this system.

We further examined pharmacological reactions of CSA-expanded human cardiomyocytes to show the relevance as cardiac cell models. We recorded field potential of re-plated beating colonies with multi-electrode array under simulation of a β-stimulant, isoproterenol, a β-blocker, propranorol, and a HERG channel inhibitor, E-4031. Addition of isoproterenol significantly increased the beating frequency (Fig. 4A), on the other hand, propranorol significantly decreased the beating frequency (Fig. 4B). E-4031 dose-dependently prolonged the length of time from the first negative peak to first positive peak, which is corresponding to QT time in electrocardiogram (Fig. 4C). These results indicate that CSA-expanded human iPSC-derived cardiomyocytes can suffice multiple functional features as human cardiomyocyte cell models.

Ultra structural features of expanded human iPSC-derived cardiomyocytes

We finally confirmed features of CSA-expanded human iPSC-derived cardiomyocytes at the ultrastructural level using electron microscopy. Beating colonies induced from human iPSCs resembled native cardiomyocytes, showing myofibrillar bundles with transverse Z-bands and enriched mitochondria (Fig. 5A-D). Other cardiomyocyte-specific structures, such as intercalated disks with desmosomes (Fig. 5D), atrial secretory granule-like structures (Fig. 5E), and glycogen granules (Fig. 5F) were also observed.

Together, these results indicate that *bona fide* human cardiomyocytes can be successfully induced and expanded from human iPSCs with this method.

Discussion

Here we demonstrated the induction and expansion of cardiac progenitors and functional cardiomyocytes from iPSCs using potent and specific effect of CSA. Human cardiomyocytes with multiple expected structural and functional features could be induced with this method. This method provides a critical technological basis to obtain cardiac cells from human iPSCs.

We have demonstrated previously that CSA treatment is most effective in inducing FCV cardiac progenitor cells, the nearest upstream of cardiomyocytes in mouse ESCs [11]. Here we showed that CSA effects on FCV cardiac progenitor and cardiomyocyte induction were also completely reproduced in mouse iPSCs. Moreover, CSA also showed significant enhancing effects of cardiomyocyte differentiation from human iPSCs in the END-2 system. This is the first report to show the effect of CSA in human stem cells. In this study, we examined four human iPSC clones, 201B6, B7 (induced with four factors) [1], 253G1 and G4 (induced without c-myc) [32]. Though the basal efficiency of cardiomyocyte differentiation from 201B6, B7 and 253G4 were lower than that from 253G1, CSA treatment significantly enhanced cardiomyocyte appearance similarly in all these human iPSC clones (Figure S1). Thus, CSA robustly induced cardiogenic differentiation in mouse ESCs, iPSCs and human iPSCs regardless their species and derivation methods.

The molecular mechanisms conducting this potent CSA effect on cardiac lineage is important, but still it is unknown. Though we examined another calcineurin inhibitor, FK506, and a NF-AT inhibitor, 11R-VIVIT, both of them did not reproduce the effect of CSA [11], indicating that the cardiogenic CSA effect is mediated by other molecular target than immunosuppressing effect of CSA. Further elucidation of molecular mechanisms of CSA in cardiomyocyte differentiation would be critical for the exploration of cardiomyocyte differentiation and regeneration strategies.

CSA-expanded cardiomyocytes from human iPSCs exhibited many features sufficing as functional cardiomyocytes. Cardiomyocytes with pacemaker-like or ventricular-like action potentials were successfully induced. Nevertheless, they were still immature compared with mature adult cardiomyocytes [36], [37] and they

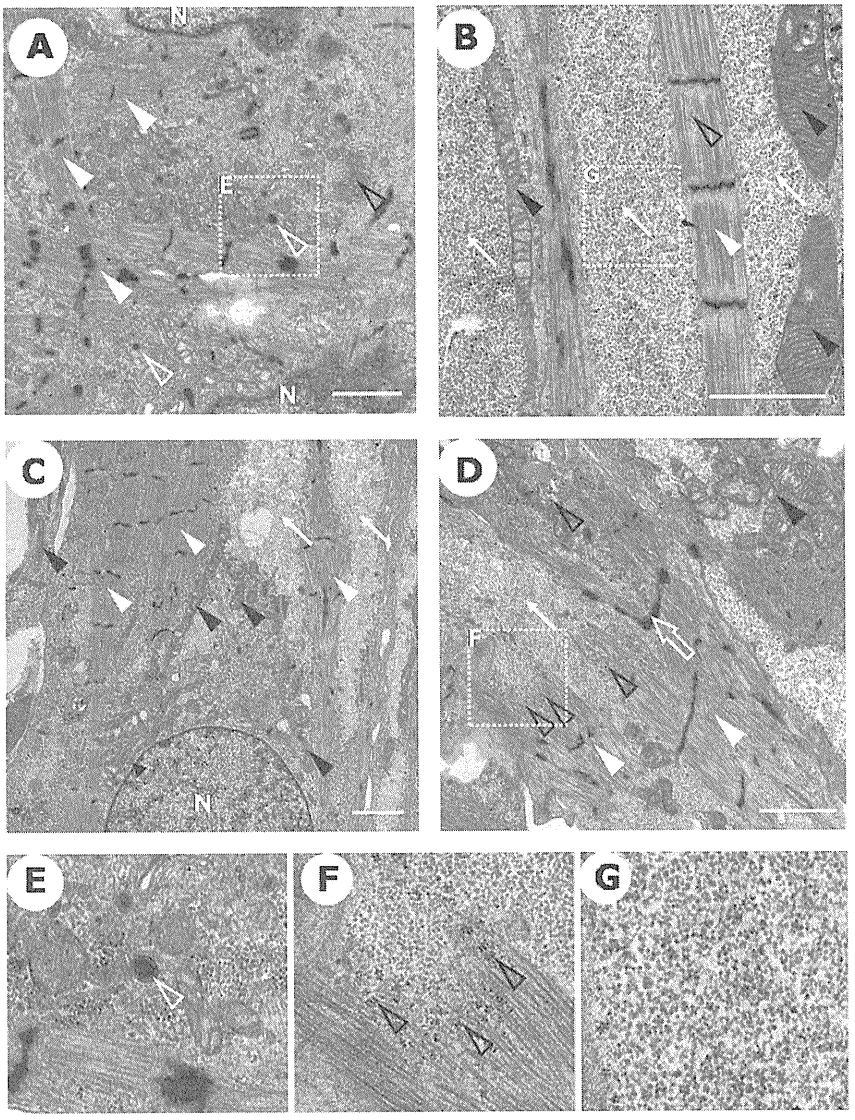

Figure 5. Ultrastructural analysis of human iPSC-derived cardiomyocytes. Transmission electron microscopic images of beating colonies. Myofibrils with Z-bands (white closed arrowheads in **A–D.**), mitochondria (black closed arrowheads in **B–D.**), intercalated disk-like structure with desmosome (white open arrow in **D.**), atrial sercetory granules (electron-dense granules surrounded by double membranes. White open arrowheads in **A.** and **E.** (magnified image of **A.**)), glycogen granules (electron-dense small granules. Black open arrowheads in **D.** and **F.** (magnified image of **D.**)), ribosomal granules (electron-lucent small granules. White arrows in **B–D.** and **G.** (magnified image of **B.**)). N: nucleus. Scale bar = 2 μm, direct magnify, ×3000 (A), ×7000 (B), ×4000 (C), ×5000 (D).
doi:10.1371/journal.pone.0016734.g005

also displayed some structural features of fetal cardiomyocytes, such as relatively low global electron density, sparse myofibrils, and abundant ribosome granules (Fig. 5). Methods for further maturation as well as specific induction and purification of the various cardiac cell types (pacemaker, atrial, ventricular, conduction system cells etc.) should be explored in future study.

Interestingly, a recent clinical report showed that CSA prevented cardiac reperfusion injury by protecting cardiomyocytes from apoptosis [38]. Cardiogenic effects of CSA in later stages of differentiation of human iPSCs imply that CSA may positively affect on endogenous cardiac progenitors to induce cardiac regeneration in patients. Though it is still unknown whether endogenous cardiac regeneration can be induced by CSA administration, our study may offer a scientific basis to support a clinical opportunity for CSA as a cardiac regenerative drug.

This novel cardiac cell differentiation method for iPSCs would thus broadly contribute to cardiac regenerative medicine by providing various options for cell preparation, transplantation strategies, and drug discovery.

Supporting Information

Figure S1 Quantitative evaluation of beating colony appearance in iPSC clones. 201B6 cells: Total colony count (control; 203±6.4/well (12-well dishes)(n = 3), CSA; 193±4.0/well (n = 3); N.S., p = 0.0915), beating colony count (control; 4.0±1.0/well (n = 3), CSA; 13.7±3.5/well (n = 3); *, $p<0.05$), percentages of beating colonies (control; 2.0±0.5% (n = 3), CSA; 7.1±1.7% (n = 3); **, $p<0.01$) in total colonies that appeared at END2-d12. 201B7 cells: Total colony count (control; 204±8.3/well (n = 3),

CSA; 200±2.0/well (n = 3); N.S., p = 0.43), beating colony count (control; 5.0±1.0/well (n = 3), CSA; 18.3±3.1/well (n = 3); **, p<0.01), percentages of beating colonies (control; 2.5±0.6% (n = 3), CSA; 9.2±1.5% (n = 3); **, p<0.01). 253G4 cells: Total colony count (control; 201±4.0/well (n = 3), CSA; 201±3.8/well (n = 3); N.S., p = 0.9216), beating colony count (control; 4.7±0.6/well (n = 3), CSA; 15.0±1.0/well (n = 3); **, p<0.05), percentages of beating colonies (control; 2.3±0.3% (n = 3), CSA; 7.5±0.6% (n = 3); †, p<0.001)
(TIF)

Movie S1 A beating colony induced from human iPS cells at END2-d12 (Fig. 2A).
(MOV)

Movie S2 A dissociated beating colony induced from human iPS cells on END-2 cells (Fig. 2H).
(MOV)

Movie S3 Real time monitoring of Ca^{++} transient by Fluo-8 in dissociated beating colony induced from human iPS cells (Fig. 3A). Clear and synchronized Ca^{++} transient is observed.
(MOV)

Table S1 Primers for PCR.
(RTF)

Acknowledgments

We thank Dr. D. Ward (Leiden University Medical Center) for supplying END-2 cells, Dr. G. Takemura (Gifu University Graduate School of Medicine) for interpretation and evaluation of electron micrograph, Novartis Pharma for providing cyclosporin-A, Dr. M. Takahashi (Kyoto University Graduate School of Medicine) for critical reading of the manuscript.

Author Contributions

Conceived and designed the experiments: MF PY JKY. Performed the experiments: MF PY TGO GN HU HF HM SM. Analyzed the data: MF TI CLM JKY. Contributed reagents/materials/analysis tools: KO KT MN CLM. Wrote the paper: MF RS CLM NN KN SY JKY.

References

1. Takahashi K, Tanabe K, Ohnuki M, Narita M, Ichisaka T, et al. (2007) Induction of pluripotent stem cells from adult human fibroblasts by defined factors. Cell 131: 861–872.
2. Takahashi K, Yamanaka S (2006) Induction of pluripotent stem cells from mouse embryonic and adult fibroblast cultures by defined factors. Cell 126: 663–676.
3. Yamanaka S (2007) Strategies and new developments in the generation of patient-specific pluripotent stem cells. Cell Stem Cell 1: 39–49.
4. Nishikawa S, Goldstein RA, Nierras CR (2008) The promise of human induced pluripotent stem cells for research and therapy. Nat Rev Mol Cell Biol 9: 725–729.
5. Reinecke H, Minami E, Zhu WZ, Laflamme MA (2008) Cardiogenic differentiation and transdifferentiation of progenitor cells. Circ Res 103: 1058–1071.
6. Laflamme MA, Murry CE (2005) Regenerating the heart. Nat Biotechnol 23: 845–856.
7. Passier R, Oostwaard DW, Snapper J, Kloots J, Hassink RJ, et al. (2005) Increased cardiomyocyte differentiation from human embryonic stem cells in serum-free cultures. Stem Cells 23: 772–780.
8. Yamashita JK, Takano M, Hiraoka-Kanie M, Shimazu C, Peishi Y, et al. (2005) Prospective identification of cardiac progenitors by a novel single cell-based cardiomyocyte induction. FASEB J 19: 1534–1536.
9. Kattman SJ, Huber TL, Keller GM (2006) Multipotent Flk-1^+ cardiovascular progenitor cells give rise to the cardiomyocyte, endothelial, and vascular smooth muscle lineages. Dev Cell 11: 723–732.
10. Fukuda K, Yuasa S (2006) Stem cells as a source of regenerative cardiomyocytes. Circ Res 98: 1002–1013.
11. Yan P, Nagasawa A, Uosaki H, Sugimoto A, Yamamizu K, et al. (2009) Cyclosporin-A potently induces highly cardiogenic progenitors from embryonic stem cells. Biochem Biophys Res Commun 379: 115–120.
12. Narazaki G, Uosaki H, Teranishi M, Okita K, Kim B, et al. (2008) Directed and systematic differentiation of cardiovascular cells from mouse induced pluripotent stem cells. Circulation 118: 498–506.
13. Mauritz C, Schwanke K, Reppel M, Neef S, Katsirntaki K, et al. (2008) Generation of functional murine cardiac myocytes from induced pluripotent stem cells. Circulation 118: 507–517.
14. Schenke-Layland K, Rhodes KE, Angelis E, Butylkova Y, Heydarkhan-Hagvall S, et al. (2008) Reprogrammed mouse fibroblasts differentiate into cells of the cardiovascular and hematopoietic lineages. Stem Cells 26: 1537–1546.
15. Zhang J, Wilson GF, Soerens AG, Koonce CH, Yu J, et al. (2009) Functional cardiomyocytes derived from human induced pluripotent stem cells. Circ Res 104: e30–41.
16. Tanaka T, Tohyama S, Murata M, Nomura F, Kaneko T, et al. (2009) In vitro pharmacologic testing using human induced pluripotent stem cell-derived cardiomyocytes. Biochem Biophys Res Commun 385: 497–502.
17. Yokoo N, Baba S, Kaichi S, Niwa A, Mima T, et al. (2009) The effects of cardioactive drugs on cardiomyocytes derived from human induced pluripotent stem cells. Biochem Biophys Res Commun 387: 482–488.
18. Zwi L, Caspi O, Arbel G, Huber I, Gepstein A, et al. (2009) Cardiomyocyte differentiation of human induced pluripotent stem cells. Circulation 120: 1513–1523.
19. Moretti A, Bellin M, Jung CB, Thies TM, Takashima Y, et al. (2010) Mouse and human induced pluripotent stem cells as a source for multipotent $Isl1^+$ cardiovascular progenitors. FASEB J 24: 700–711.
20. Yamashita J, Itoh H, Hirashima M, Ogawa M, Nishikawa S, et al. (2000) Flk1-positive cells derived from embryonic stem cells serve as vascular progenitors. Nature 408: 92–96.
21. Nishikawa SI, Nishikawa S, Hirashima M, Matsuyoshi N, Kodama H (1998) Progressive lineage analysis by cell sorting and culture identifies $FLK1^+VE$-$cadherin^+$ cells at a diverging point of endothelial and hemopoietic lineages. Development 125: 1747–1757.
22. Kataoka H, Takakura N, Nishikawa S, Tsuchida K, Kodama H, et al. (1997) Expressions of PDGF receptor alpha, c-Kit and Flk1 genes clustering in mouse chromosome 5 define distinct subsets of nascent mesodermal cells. Dev Growth Differ 39: 729–740.
23. Yamashita J (2004) Cardiovascular cell differentiation from ES cells. In: Mori H, Matsuda H, eds. Cardiovascular Regeneration Therapies Using Tissue Engineering Approaches. Tokyo: Springer-Verlag GmbH, Chapter 2. pp 67–80.
24. Moretti A, Caron L, Nakano A, Lam JT, Bernshausen A, et al. (2006) Multipotent embryonic $isl1^+$ progenitor cells lead to cardiac, smooth muscle, and endothelial cell diversification. Cell 127: 1151–1165.
25. Wu SM, Fujiwara Y, Cibulsky SM, Clapham DE, Lien CL, et al. (2006) Developmental origin of a bipotential myocardial and smooth muscle cell precursor in the mammalian heart. Cell 127: 1137–1150.
26. Garry DJ, Olson EN (2006) A common progenitor at the heart of development. Cell 127: 1101–1104.
27. Yamashita JK (2007) Differentiation of arterial, venous, and lymphatic endothelial cells from vascular progenitors. Trends Cardiovasc Med 17: 59–63.
28. Yamashita JK (2004) Differentiation and diversification of vascular cells from embryonic stem cells. Int J Hematol 80: 1–6.
29. Yanagi K, Takano M, Narazaki G, Uosaki H, Hoshino T, et al. (2007) Hyperpolarization-activated cyclic nucleotide-gated channels and T-type calcium channels confer automaticity of embryonic stem cell-derived cardiomyocytes. Stem Cells 25: 2712–2719.
30. Okita K, Ichisaka T, Yamanaka S (2007) Generation of germline-competent induced pluripotent stem cells. Nature 448: 313–317.
31. Mummery C, Ward-van Oostwaard D, Doevendans P, Spijker R, van den Brink S, et al. (2003) Differentiation of human embryonic stem cells to cardiomyocytes: role of coculture with visceral endoderm-like cells. Circulation 107: 2733–2740.
32. Nakagawa M, Koyanagi M, Tanabe K, Takahashi K, Ichisaka T, et al. (2008) Generation of induced pluripotent stem cells without Myc from mouse and human fibroblasts. Nat Biotechnol 26: 101–106.
33. Yamamizu K, Kawasaki K, Katayama S, Watabe T, Yamashita JK (2009) Enhancement of vascular progenitor potential by protein kinase A through dual induction of Flk-1 and Neuropilin-1. Blood 114: 3707–3716.
34. Yang L, Soonpaa MH, Adler ED, Roepke TK, Kattman SJ, et al. (2008) Human cardiovascular progenitor cells develop from a KDR^+ embryonic-stem-cell-derived population. Nature 453: 524–528.
35. Sone M, Itoh H, Yamahara K, Yamashita JK, Yurugi-Kobayashi T, et al. (2007) Pathway for differentiation of human embryonic stem cells to vascular cell components and their potential for vascular regeneration. Arterioscler Thromb Vasc Biol 27: 2127–2134.
36. Chacko KJ (1976) Observations on the ultrastructure of developing myocardium of rat embryos. J Morphol 150: 681–709.
37. Kehat I, Kenyagin-Karsenti D, Snir M, Segev H, Amit M, et al. (2001) Human embryonic stem cells can differentiate into myocytes with structural and functional properties of cardiomyocytes. J Clin Invest 108: 407–414.
38. Piot C, Croisille P, Staat P, Thibault H, Rioufol G, et al. (2008) Effect of cyclosporine on reperfusion injury in acute myocardial infarction. N Engl J Med 359: 473–481.

LIVER TRANSPLANTATION 17:144-148, 2011

ORIGINAL ARTICLE

Immediate Noninvasive Ventilation May Improve Mortality in Patients With Hepatopulmonary Syndrome After Liver Transplantation

Yuichi Chihara,[1] Hiroto Egawa,[4] Tomomasa Tsuboi,[5] Toru Oga,[5] Tomohiro Handa,[2] Kazuhiko Yamamoto,[6] Michiaki Mishima,[1] Koichi Tanaka,[7] Shinji Uemoto,[3] and Kazuo Chin[5]

Departments of [1]Respiratory Medicine, [2]Rehabilitation, and [3]Transplant Surgery, Kyoto University Hospital, Kyoto, Japan; [4]Department of Surgery, Murakami Memorial Hospital, Asahi University, Gifu, Japan; Departments of [5]Respiratory Care and Sleep Control Medicine, Kyoto University Graduate School of Medicine, Kyoto, Japan; Departments of [6]Allergy and Rheumatology, Tokyo University Graduate School of Medicine, Tokyo, Japan; and [7]Foundation for Biomedical Research and Innovation, Kobe, Japan

Hepatopulmonary syndrome (HPS) is defined as hypoxemia induced by intrapulmonary vascular dilations associated with liver disease. Although liver transplantation (LT) is the only effective therapy established for severe HPS, patients with a partial pressure of arterial oxygen (PaO_2) less than 60 mm Hg have a poor prognosis. We treated a 4-year-old boy with HPS whose preoperative PaO_2 level was 48.8 mm Hg. After LT, he had persistent severe hypoxemia, although he was receiving high-flow oxygen. Noninvasive ventilation (NIV) was introduced, and his respiratory insufficiency promptly improved. Therefore, NIV therapy immediately after extubation following transplantation was administered to the next 4 consecutive HPS patients whose preoperative PaO_2 was less than 60 mm Hg. The NIV treatment of these 5 patients could have been responsible for preventing severe postoperative complications as well as reintubation and hospital death. NIV therapy for both pediatric and adult patients with severe HPS immediately after extubation might protect them from severe hypoxemia after transplantation and from complications necessitating reintubation and might improve their prognosis. ***Liver Transpl 17:144-148, 2011.*** © **2011 AASLD.**

Received July 6, 2010; accepted October 5, 2010.

Hepatopulmonary syndrome (HPS) is defined as a defect in arterial oxygenation induced by intrapulmonary vascular dilations associated with liver disease.[1] Previous studies have determined that HPS is an independent risk factor for long-term mortality in patients with cirrhosis.[2]

Orthotopic liver transplantation (OLT) is the only successful treatment for patients with HPS. However, the postoperative mortality rate of patients with severe hypoxemia before transplantation has been high.[3] Patients with a partial pressure of arterial oxygen (PaO_2) less than or equal to 60 mm Hg have been shown to have a poor prognosis after liver transplantation (LT), and a baseline PaO_2 less than or equal to 50 mm Hg has been associated with a poor survival rate, regardless of the decision to perform OLT.[2] Indeed, at

Abbreviations: $AaDO_2$, alveolar-arterial oxygen gradient; F_IO_2, fraction of inspired oxygen; HCV-LC, hepatitis C virus–related liver cirrhosis; HPS, hepatopulmonary syndrome; LDLT, living donor liver transplantation; LT, liver transplantation; NIV, noninvasive ventilation; OLT, orthotopic liver transplantation; $PaCO_2$, partial pressure of arterial carbon dioxide; PaO_2, partial pressure of arterial oxygen; P_AO_2, partial pressure of alveolar oxygen; P_{atm}, atmospheric pressure; PH_2O, partial pressure of water vapor at body temperature; POD, postoperative day; SaO_2, arterial oxygen saturation; SpO_2, percutaneous oxygen saturation; ST, spontaneous/timed; *X*, leakage flow rate; *Y*, oxygen flow rate.

This work was supported by grants from the Japanese Ministry of Education, Culture, Sports, Science, and Technology (20590921 and 22590860); by the Respiratory Failure Research Group; by health sciences research grants (Comprehensive Research on Life-Style Related Diseases Including Cardiovascular Diseases and Diabetes Mellitus) from the Japanese Ministry of Health, Labor, and Welfare; and by the Japan Vascular Disease Research Foundation.

Address reprint requests to Kazuo Chin, M.D., Ph.D., Department of Respiratory Care and Sleep Control Medicine, Kyoto University Graduate School of Medicine, Kyoto University Hospital, 54 Shogoin Kawahara- Cho, Sakyo-Ku, Kyoto 606-8507, Japan. Telephone: 81-75-751-3852; FAX: 81-75-751-3854; E-mail: chink@kuhp.kyoto-u.ac.jp

DOI 10.1002/lt.22207
View this article online at wileyonlinelibrary.com.
LIVER TRANSPLANTATION.DOI 10.1002/lt. *Published on behalf of the American Association for the Study of Liver Diseases*

TABLE 1. Preoperative Status of Five Cases

	Case 1	Case 2	Case 3	Case 4	Case 5
Age (years)	4	60	10	11	59
Sex	Male	Male	Female	Female	Male
Etiology	Biliary atresia	HCV-LC	Biliary atresia	Congenital absence of the portal vein	HCV-LC
Preoperative PaO_2 (mm Hg)	48.8	49.3	50	61.6 (2 L/minute by a nasal cannula)	57.5
Preoperative $AaDO_2$ (mm Hg)*	67.4	60.1	62.5	95.7†	58.0
Preoperative shunt ratio (%)	43.6	45	42.3	42	35.9
Child-Pugh class	A	C	A	A	C
Model for End-Stage Liver Disease score	9	17	10	11	17
LT date	July 2003	March 2005	December 2005	June 2006	October 2007
Blood group with graft	Identical	Identical	Identical	Compatible	Identical

*$AaDO_2$ ($PAO_2 - PaO_2$) = $F_IO_2(P_{atm} - PH_2O) - (PaCO_2/0.8) - PaO_2$.
†F_IO_2 for this case was determined to be 0.28.[12]

our institute, 6 of 14 patients with severe HPS (ie, patients with $PaO_2 < 60$ mm Hg, including 11 cases with $PaO_2 \leq 50$ mm Hg on room air) died in the hospital after living donor liver transplantation (LDLT).[4]

Noninvasive ventilation (NIV) is effective for respiratory insufficiency in many situations (eg, after organ transplantation).[5] However, there has been no previous report on the use of NIV after LT in patients with severe HPS.

Here we report the details of successful postoperative management with NIV treatment of 5 consecutive patients with severe HPS.

PATIENTS AND METHODS

Patients

From July 2003 to March 2009, 5 consecutive patients with severe HPS whose PaO_2 on room air was less than 60 mm Hg were under respiratory management with NIV during the perioperative period of LT. The preoperative status of these 5 patients is shown in Table 1. Although the use of NIV was unplanned in case 1, NIV was planned to be applied immediately after LDLT in the other 4 cases. However, 90 minutes passed before the introduction of NIV after extubation in case 3 because of a delay in medical orders. In case 4, the preoperative PaO_2 level was 61.6 mm Hg while the patient was receiving 2 L of oxygen per minute via a nasal cannula. Therefore, her PaO_2 level was presumed to be less than 50 mm Hg on room air because the fraction of inspired oxygen (F_IO_2) was presumed to be greater than 0.28 while she was receiving 2 L of oxygen per minute via the nasal cannula.[6] With the inclusion of case 4, PaO_2 in 4 of the 5 patients with HPS was less than or equal to 50 mm Hg while the patients were breathing room air. The preoperative shunt ratio, estimated with a technetium-99m macroaggregated albumin lung perfusion scan, was more than 40% in 4 of the 5 patients (Table 1).

After LT, the discontinuation of mechanical ventilation was considered under the following conditions, which were the same as those before the introduction of NIV treatment at our institution: (1) the patient was clinically stable, (2) the underlying disease and its complications had improved, (3) ventilator support was minimal (pressure support $\leq$ 6 cm H_2O and positive end-expiratory pressure $\leq$ 4 cm H_2O), and (4) spontaneous breathing was sufficient. When the patients were extubated, F_IO_2 of the ventilator settings ranged from 0.4 to 0.65, and the PaO_2/F_IO_2 ratio was greater than 100. The ethics committee of Kyoto University gave its approval for the protocol of this study.

Oxygen Therapy and NIV

For the estimation of F_IO_2 of oxygen therapy via a nasal cannula, face mask, or reservoir face mask, we calculated F_IO_2 with a previously published formula.[6] During NIV treatment, we used a full-face mask, a nasal mask (Resmed, North Ryde, New South Wales, Australia), or a nasal mask of pediatric size (Respironics, Murrysville, PA).

A bilevel positive airway pressure device (VPAP II ST-A, Resmed), supplemental oxygen, and a heated humidifier were used. At first, we used a full-face mask as an interface. After the mask had been secured, the level of support pressure, the expiratory positive airway pressure, and the amount of oxygen were progressively increased until the arterial oxygen saturation (SaO_2) was greater than 95%, and this was accompanied by decreased respiratory rates and/or reduced activity of accessory muscles for respiration, decreased paradoxical thoracoabdominal movement, and an improvement in the patient's respiratory discomfort. When NIV was being introduced, a doctor stayed at the bedside and observed the patient carefully while the SaO_2 levels and electrocardiogram were monitored. Throughout the first hour, the patient's condition was assessed repeatedly. To stabilize the patient's respiratory status, adjustments were made in NIV settings and oxygen.

TABLE 2. Initial Setting of NIV in Five Cases

	Case 1	Case 2	Case 3	Case 4	Case 5
Mode	ST	ST	ST	ST	ST
Inspiratory positive airway pressure (cm H_2O)	5.6	11	8	11.2	8
Expiratory positive airway pressure (cm H_2O)	3.6	5	4	5.2	4
Respiratory rate (breaths/minute)	30	14	14	16	12
Amount of oxygen (L/minute)	15	15	12	15	8
Interface	Face mask	Face mask	Face mask	Face mask	Face mask

When NIV was initially applied, the goal was to continue its use as long as the patient could tolerate it or until it appeared to no longer be necessary. After the respiratory status was stabilized, some patients (cases 2 and 3) continued to use the nasal mask to avoid aspiration after vomiting. To prevent abdominal distension and vomiting, a gastric tube was inserted into the stomach on either the first or second day of NIV introduction in cases 2 to 5. When the SaO_2 levels were greater than 90% with the delivery of 5 L of oxygen per minute through a nasal cannula or mask, NIV was discontinued during awake periods, and the NIV settings (pressure and amount of oxygen) were gradually lowered. However, in case 3, NIV was discontinued while her SaO_2 levels were less than 90% but more than 85% because she insisted on stopping NIV as soon as possible.

To calculate F_IO_2 during NIV, we used the information supplied by the manufacturer and attached to the mask. With this information, F_IO_2 was determined from the following parameters: the leakage flow per minute from the mask at each pressure and the oxygen flow per minute during NIV. With X as the leakage flow rate and Y as the oxygen flow rate in this setting, F_IO_2 in this setting was calculated as follows:

$$F_IO_2 = [Y \times 1.0 + (X - Y) \times 0.21]/X$$

Whenever respiratory conditions deteriorated, invasive mechanical ventilation was applied. The predetermined criteria for reintubation were as follows: the failure to maintain an SaO_2 level less than 90% with F_IO_2 equal to or greater than 0.6, the development of conditions necessitating endotracheal intubation to protect the upper airway (seizure and severe hepatic coma), the development of copious tracheal secretions that could not be expectorated, an increase in the partial pressure of arterial carbon dioxide ($PaCO_2$) accompanied by a pH less than or equal to 7.30, and severe hemodynamic instability defined as a systolic blood pressure less than 70 mm Hg.

RESULTS

Case 1

Case 1 was a 4-year-old boy with biliary atresia. His preoperative PaO_2 level while he was breathing room air was 48.8 mm Hg, and his shunt ratio was 43.6% (Table 1). He underwent LDLT with an ABO-identical graft. On postoperative day (POD) 1, the patient was extubated. We could not keep his percutaneous oxygen saturation (SpO_2) greater than 90% even while he was inhaling high-flow oxygen (10 L/minute) with a reservoir face mask. We started NIV treatment on POD 9 (Table 2). After the introduction of NIV, within 6 hours, the PaO_2/F_IO_2 ratio and respiratory rate improved from 75.4 to 179.2 and from 45 to 34 breaths/minute, respectively (Table 3). On POD 12, NIV with oxygen was changed to the nocturnal use of NIV with oxygen and diurnal oxygen therapy. NIV was discontinued on POD 34, and oxygen therapy was stopped on POD 74. The patient was discharged from our hospital on POD 83 and remains alive.

Case 2

Case 2 was a 60-year-old man with hepatitis C virus–related liver cirrhosis (HCV-LC). His preoperative PaO_2 level while he was breathing room air was 49.3 mm Hg, and his shunt ratio was 45% (Table 1). After LDLT with an ABO-identical graft, extubation was executed on POD 2. Because of our experience with case 1, we started NIV immediately after extubation. We used NIV continuously all day, and his SpO_2 level was well controlled (Table 3). On POD 9, the patient received 1 hour of NIV 3 times per day because he refused to use NIV continuously. On POD 20, we were able to discontinue NIV, and the patient was discharged from our hospital on POD 33. He died 5 months after LDLT because of the rupture of a thoracic aortic aneurysm.

Case 3

Case 3 was a 10-year-old girl with biliary atresia. Because of her low PaO_2 level before transplantation, the patient started NIV with both face and nasal masks a few days before the operation. On POD 1, she was extubated. We introduced NIV 90 minutes after extubation, and her oxygenation improved (Table 3). From POD 12, the nocturnal use of NIV controlled her SpO_2 level well, but diurnally, severe hypoxemia with an elevated heart rate persisted despite the administration of high-flow oxygen with a reservoir face mask (Fig. 1). She wanted to discontinue NIV treatment on POD 89. However, her SpO_2 level was only 88% even

TABLE 3. Clinical Course of Five Cases

	Case 1	Case 2	Case 3	Case 4	Case 5
PaO_2/F_IO_2 before the operation	232.4	234.8	250.0	220.0*	273.8
PaO_2/F_IO_2 before extubation	101.2	107.8	138.5	186.7	289.0
Time from extubation to the introduction of NIV	8 days	Immediately	1.5 hours	Immediately	Immediately
PaO_2/F_IO_2 before NIV	75.4	107.8	73.6	186.7	289.0
PaO_2/F_IO_2 after NIV	179.2 (6 hours)	138.4 (4 hours)	177.9 (6 hours)	186.9 (3 hours)	252.9 (1 hour)
Respiratory rate before NIV (breaths/minute)	45	18	17	20	10
Respiratory rate 2 hours after NIV (breaths/minute)	34	22	15	18	14
Length of hospitalization (days)	98	33	105	51	119
Duration of NIV (days)	25	18	88	11	59
Duration of oxygen therapy (days)	74	33	171	41	63
SpO_2 on discharge (%)	99 (room air)	92 (room air)	88 (5 L/minute reservoir face mask)	97 (room air)	97 (room air)
Postoperative shunt ratio after LT (%)	14.7 (1 month)	34 (1 month)	16.5 (3 months)	7.6 (3 months)	26.0 (2 months)

*F_IO_2 for this case was determined to be 0.28.[12]

while she was breathing 5 L of oxygen per minute. She was discharged from our hospital on POD 95. Her oxygenation gradually improved over a long period, and her SpO_2 level stabilized at approximately 96% while she was breathing room air. Long-term oxygen therapy was discontinued after 171 days. She is alive, and her liver function and oxygenation have normalized.

Cases 4 and 5

Case 4 was an 11-year-old girl with congenital absence of the portal vein, and case 5 was a 59-year-old man with HCV-LC. After LDLT, both patients were extubated on POD 1, and NIV was introduced immediately. Their respiratory status stabilized, and they experienced no complications. They were discharged from our hospital and are alive.

All 5 patients with severe HPS were treated with NIV with the spontaneous/timed (ST) mode and could be discharged from the hospital after LT. After NIV was applied, the respiratory rate in case 1 improved. In contrast to case 1, the other 4 patients, who were started on NIV immediately or early after extubation, did not have severe tachypnea before extubation. These patients experienced no significant changes in their respiratory rates before and after NIV. Although case 1 had a bile leak, no other complications, including the necessity for reintubation, infection, or reoperation, were encountered in these patients. In addition, no severe complications such as pneumothorax, hypotension, or aspiration pneumonia related to the NIV treatment occurred among these 5 patients.

DISCUSSION

This is the first report showing the effectiveness of NIV treatment for hypoxemia in patients with severe HPS. The postoperative management of patients with severe HPS is said to be exceedingly difficult because HPS patients with severe hypoxemia manifest worsening of respiratory insufficiency after LT. The results of this study indicate that by controlling hypoxemia more effectively than the therapies used previously and by avoiding the need for reintubation without severe side effects, NIV after LT might improve the mortality rates of severe HPS patients.

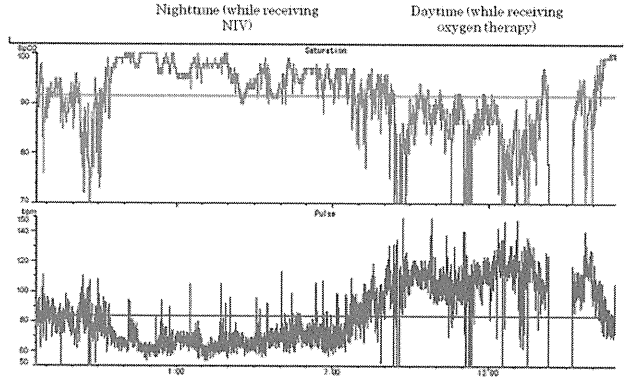

Figure 1. Changes in SpO_2 (top) and in the pulse rate (bottom) in a day. SpO_2 was higher when the patient was undergoing NIV therapy with oxygen at night than when the patient was receiving only oxygen therapy during the day. [Color figure can be viewed in the online issue, which is available at wileyonlinelibrary.com.]

The effectiveness of NIV in patients with acute respiratory failure after solid organ transplantation[5] and in the prevention of respiratory failure after extubation in high-risk patients[7] has been demonstrated. Feltracco et al.[8] reported the use of NIV in clinical practice (eg, as a tool facilitating early extubation and

as a prophylactic strategy for preventing postoperative pulmonary complications). However, that report did not examine the application of NIV for specific diseases as our study does.

Several factors are relevant to postoperative hypoxemia; these include intraoperative fluid overloading, atelectasis, and restrictive disorders due to abdominal distension and/or pleural effusion after transplantation. In addition, as a characteristic factor of hypoxemia in patients with HPS, absent or reduced pulmonary vascular tone with impaired hypoxic vasoconstriction due to HPS[9] may also contribute to postoperative hypoxemia. However, NIV could improve oxygenation despite the existence of these factors in these case series.

Recently, oxygen desaturation during sleep was reported in patients with HPS; the degree correlated with the severity of HPS.[10] NIV may prevent nocturnal hypoventilation and/or upper airway obstruction (eg, case 3; Fig. 1).

We previously reported on 21 HPS patients after LDLT in our hospital[4]; 14 had severe hypoxemia before LDLT. Although the LDLT surgical procedures and the management of infectious complications were unchanged between the 2 time periods, improvements in perioperative management, including surgical techniques, fluid management, and antibiotics, might have influenced the outcomes.

Although there was no serious ventilator-associated pneumonia resulting in hospital death in our previous studies, 11 of our 14 previous patients (78.6%) whose PaO_2 level before transplantation was less than 60 mm Hg developed serious postoperative infections, such as wound infections, sepsis derived from cholangitis, and intraperitoneal abscesses.[4,11] However, no postoperative infection occurred in the 5 cases shown here. We feel that the early improvement in oxygenation by NIV treatment might have prevented serious infectious complications in our patients.

Complications of NIV treatment such as severe skin rashes, eye irritation, gastric insufflation, and aspiration, which can necessitate the cessation of NIV treatment, were not apparent in our patients. When patients indicated discomfort from the mask or pressure, we decreased the usage time of NIV or changed to another type of mask.

This study has some limitations. First, the patient population was heterogeneous with respect to age and was small in number. The period between extubation and the introduction of NIV was also heterogeneous: NIV treatment began immediately after extubation in cases 2, 4, and 5 but not in cases 1 and 3. The PaO_2/F_IO_2 ratio before NIV in cases 1 and 3 decreased with respect to the ratio before extubation. Therefore, we propose that immediate (preventive) NIV after extubation would be more favorable in patients with severe HPS. According to Antonelli and Bello,[12] several studies have assessed the benefit of NIV in various weaning strategies, including the use of early extubation in patients who fail to meet standard extubation criteria (facilitation use), the avoidance of reintubation in patients who fail extubation (curative use), and the prevention of extubation failure in unselected and selected patients (preventive use). We propose that good results can be achieved by the preventive use of NIV in patients with HPS. However, it is impossible to determine the actual value of preventive NIV use for HPS patients without a prospective randomized trial.

In conclusion, although this study was not a randomized trial and the number of cases was small and heterogeneous, immediate NIV may possibly improve the prognosis in patients, both children and adults, with severe HPS without serious complications. We propose that this treatment be used for patients with severe HPS after LT because the control of consecutive severe hypoxemia after LT is one of the most important factors for the improvement of the prognosis of these patients.

REFERENCES

1. Rodriguez-Roisin R, Krowka MJ, Herve P, Fallon MB. Pulmonary-hepatic vascular disorders (PHD). Eur Respir J 2004;24:861-880.
2. Swanson KL, Wiesner RH, Krowka MJ. Natural history of hepatopulmonary syndrome: impact of liver transplantation. Hepatology 2005;41:1122-1129.
3. Rodriguez-Roisin R, Krowka MJ. Hepatopulmonary syndrome—a liver-induced lung vascular disorder. N Eng J Med 2008;358:2378-2387.
4. Egawa H, Kasahara M, Inomata Y, Uemoto S, Asonuma K, Fujita S, et al. Long-term outcome of living related liver transplantation for patients with intrapulmonary shunting and strategy for complications. Transplantation 1999;67:712-717.
5. Antonelli M, Conti G, Bufi M, Costa MG, Lappa A, Rocco M, et al. Noninvasive ventilation for treatment of acute respiratory failure in patients undergoing solid organ transplantation: a randomized trial. JAMA 2000;283: 235-241.
6. Shapiro BA, Harrison RA, Kacmarek RM, Cane RA. Clinical Application of Respiratory Care. 3rd ed. Chicago, IL: Year Book Medical Publishers; 1985:180-187.
7. Nava S, Gregoretti C, Fanfulla F, Squadrone E, Grassi M, Carlucci A, et al. Noninvasive ventilation to prevent respiratory failure after extubation in high-risk patients. Crit Care Med 2005;33:2465-2470.
8. Feltracco P, Serra E, Barbieri S, Milevoj M, Salvaterra F, Marulli G, Ori C. Noninvasive ventilation in adult liver transplantation. Transplant Proc 2008;40:1979-1982.
9. Rodriguez-Roisin R, Roca J, Agusti AG, Mastai R, Wagner PD, Bosch J. Gas exchange and pulmonary vascular reactivity in patients with liver cirrhosis. Am Rev Respir Dis 1987;135:1085-1092.
10. Palma DT, Philips GM, Arguedas MR, Harding SM, Fallon MB. Oxygen desaturation during sleep in hepatopulmonary syndrome. Hepatology 2008;47:1257-1263.
11. Uemoto S, Inomata Y, Egawa H, Satomura K, Kiuchi T, Okajima H, et al. Effects of hypoxemia on early postoperative course of liver transplantation in pediatric patients with intrapulmonary shunting. Transplantation 1997;63:407-414.
12. Antonelli M, Bello G. Noninvasive mechanical ventilation during the weaning process: facilitative, curative, or preventive? Crit Care 2008;12:136.

Impact of Exacerbations on Emphysema Progression in Chronic Obstructive Pulmonary Disease

Naoya Tanabe[1], Shigeo Muro[1], Toyohiro Hirai[1], Tsuyoshi Oguma[1], Kunihiko Terada[1], Satoshi Marumo[1], Daisuke Kinose[1], Emiko Ogawa[1], Yuma Hoshino[1], and Michiaki Mishima[1]

[1]Department of Respiratory Medicine, Graduate School of Medicine, Kyoto University, Kyoto, Japan

Rationale: Low-attenuation areas assessed by computed tomography reflect the extent of pathological emphysema and correlate with airflow limitation and mortality in patients with chronic obstructive pulmonary disease. The cumulative size distribution of low-attenuation area clusters follows a power law characterized by an exponent, D. The values of D reflect the complexity of the terminal airspace geometry and sensitively detect alveolar structural changes. Exacerbations of chronic obstructive pulmonary disease have a negative impact on lung function and prognosis. However, the impact on emphysema progression remains unclear.

Objectives: We investigated the relationship between exacerbation and emphysema progression assessed by computed tomography in patients with chronic obstructive pulmonary disease.

Methods: Exacerbations were prospectively recorded for 2 years. Annual changes in computed tomography parameters of emphysema were compared between patients with and without a history of exacerbations.

Measurements and Main Results: In patients with exacerbations, increases in the percentage of low-attenuation areas and decreases in D were greater than in patients without exacerbations. To interpret these results, we established a novel simulation model and found that not only enlargement of preexisting low-attenuation areas but also coalescence of adjoining low-attenuation areas due to alveolar wall destruction caused emphysema progression in patients with exacerbations.

Conclusions: This is the first longitudinal study to demonstrate that exacerbations are involved in emphysema progression in patients with chronic obstructive pulmonary disease. Emphysema progression should be evaluated as part of the outcomes of exacerbations in the management of chronic obstructive pulmonary disease.

Keywords: emphysema; exacerbation; computed tomography; chronic obstructive pulmonary disease; fractal

AT A GLANCE COMMENTARY

Scientific Knowledge on the Subject

Pulmonary emphysema is the primary pathological change of chronic obstructive pulmonary disease (COPD) and can be assessed by computed tomography (CT). Exacerbations of COPD have a negative impact on lung function and prognosis. However, the relationship between exacerbations and progression of emphysema remains unclear.

What This Study Adds to the Field

This study shows that annual changes in CT parameters of emphysema are greater in patients with a history of exacerbations of COPD than in those without a history of exacerbations. This finding suggests that exacerbations accelerate emphysema progression in patients with COPD.

Chronic obstructive pulmonary disease (COPD) is a major public health problem. It is the fourth leading cause of death worldwide and is associated with increasing economic costs and social burdens (1). Emphysema, a main constituent of lung pathology in COPD, is characterized pathologically by abnormal and permanent enlargement of distal airspaces and destruction of alveolar walls (2). It causes airflow limitations (3) and impaired diffusing capacities (4), which are important determinants of COPD mortality. Investigating the mechanism of emphysema progression is therefore important to improve management of patients with COPD.

Exacerbations of COPD consist of acute episodes of worsening symptoms that may warrant changes in regular medications (1) and lead to worsening of the chronic progressive course of this disease. These exacerbations have negative impacts on lung function (5), health-related quality of life (6, 7), prognosis (8), and socioeconomic costs (9). However, it is not clear whether exacerbations of COPD promote emphysema progression.

Computed tomography (CT) has been previously used to assess the extent of emphysematous changes (3, 4, 10–14). The loss of lung tissue associated with emphysema can be measured by low-attenuation areas (LAA) in CT images, and the importance of such assessments of emphysematous changes is increasingly being recognized in clinical practice. In patients with α_1-antitrypsin deficiency, emphysematous changes assessed by CT are more sensitive for detecting the efficacy of augmentation therapy than other conventional indices such as lung function tests (15). In typical patients with COPD, emphysematous changes assessed by CT are correlated with COPD mortality, independently of lung function (16). This finding suggests that CT assessment of emphysematous changes can provide additional information for managing patients with COPD.

The concept of fractal geometry is useful for analyzing the irregular and complex structures often seen in nature (17), and it has been applied to pulmonary physiology and histology (18, 19). We previously demonstrated that the cumulative size dis-

(*Received in original form September 24, 2010; accepted in final form March 10, 2011*)

Supported by grants-in-aid for scientific research (B) (no. 16390234) and (C) (no. 21590964) and a grant to the Respiratory Failure Research Group from the Ministry of Health, Labor, and Welfare, Japan.

Author contribution: N.T. contributed to study design, collection of data, analysis and interpretation of data, and writing the draft. S.M. contributed to study design, collection of data, analysis and interpretation of data, editing the draft, and acquisition of funding. T.H. contributed to the development of computer simulation analysis, editing the draft, and interpretation of data. T.O. developed the custom-made application for the analysis of computed tomography data, and contributed to interpretation of data and editing the draft. K.T. contributed to study design, collection of data, and analysis. S.M. contributed to study design, collection of data, and analysis. D.K. contributed to study design, collection of data, and analysis. E.O. contributed to study design, collection of data, and analysis. Y.H. contributed to study design, collection of data, and analysis. M.M. contributed to study design and analysis and interpretation of data, editing the draft, and acquisition of funding.

Correspondence and requests for reprints should be addressed to Shigeo Muro M.D., Ph.D., Department of Respiratory Medicine, Graduate School of Medicine, Kyoto University, 53 Kawahara-cho, Shogoin, Sakyo-ku, Kyoto 606-8507, Japan. E-mail: smuro@kuhp.kyoto-u.ac.jp

This article has an online supplement, which is available from this issue's table of contents at www.atsjournals.org

Am J Respir Crit Care Med Vol 183. pp 1653–1659, 2011
Originally Published in Press as DOI: 10.1164/rccm.201009-1535OC on March 11, 2011
Internet address: www.atsjournals.org

tribution of LAA clusters follows a power law characterized by an exponent, D. The values of D reflect the fractal dimension of the terminal airspace geometry, and could be sensitive to alterations in tissue structure that are not reflected in changes in the percentage of the lung field occupied by LAAs (LAA%) (4). Moreover, we also found that fractal analysis is useful in elucidating the mechanism of emphysema progression in an animal model (20). These reports suggest that the evaluation of LAA and fractal geometry could reveal faint alterations in lung structure in the clinical course of patients with COPD.

In the present study, we explored the impact of COPD exacerbations on emphysema progression by analyzing changes in both LAA% and D. We then investigated the underlying mechanism by establishing a novel simulation model.

METHODS

This is part of a prospective observational study investigating COPD exacerbation (21–23). The study protocol is summarized in Figure 1, and details of all protocols are provided in the online supplement. Briefly, from June 2006 to August 2008, we enrolled 101 of 105 patients with COPD who agreed to record exacerbations prospectively. The observation period was 2 years. The study was approved by the local ethics committee, and all patients gave written informed consent.

Exacerbation Criteria

We defined an exacerbation as a symptomatic deterioration requiring treatment with antibiotics and/or systemic corticosteroid. As previously reported (21–23), symptomatic changes were assessed by a modified version of the East London Cohort Study criteria (5, 6).

Pulmonary Function Tests, CT Acquisition, and Calibration of CT Numbers

As previously reported (24, 25), baseline and 2-year follow-up pulmonary function tests and CT scans were performed at least 4 weeks after resolution of the last exacerbation. In addition to routine calibration using air and water phantoms, CT numbers were corrected using air densities sampled from the intrathoracic trachea to eliminate the influence of X-ray tube aging (26).

Analysis of the Percentage of LAA and the Cumulative Frequency Distribution of LAA Size

We measured CT parameters according to our previous reports (4, 25). The cumulative frequency distribution of LAA sizes, Y, can be described by a power law of LAA size X of the form: $Y = K \times X^{-D}$. Using all images of the whole lung (slice thickness, 0.5 mm), we calculated the values of LAA%, exponent D, and CT-derived lung volume.

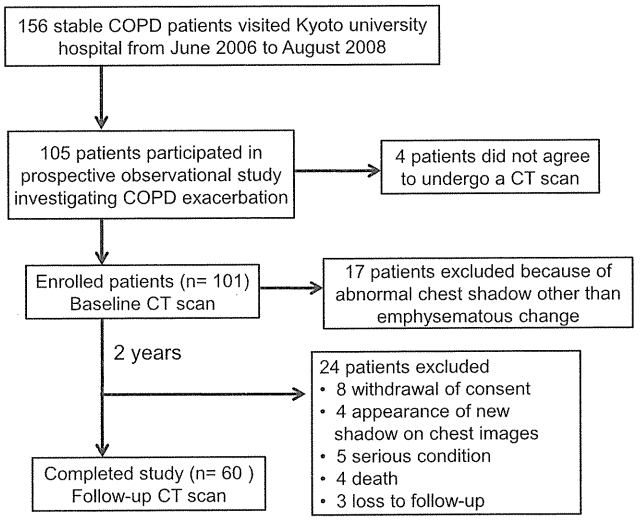

Figure 1. Patient disposition and reasons for exclusion. CT = computed tomography; COPD = chronic obstructive pulmonary disease.

Model Simulations

We established a simulation model using baseline CT images (*see* Figure E1 in the online supplement). One pixel in each image was randomly selected from the boundary of preexisting LAAs and changed into a new LAA pixel. This process was iteratively repeated, using the modified image as the starting point for the next selection until changes in LAA% reached 1, 3, and 5%. The procedure was performed according to various algorithms as follows. In model A, one pixel was randomly selected from all pixels in the boundary of LAAs, but not separating adjoining LAAs. This model simulates the simple enlargement of preexisting LAA. In model B, either 15% (model B15) or 30% (model B30) of pixels were randomly selected from all pixels separating LAAs, and then the remaining pixels were randomly selected from all those in the boundary of LAAs, but not separating LAAs. Model B simulates the situation in which lung destruction causes the coalescence of neighboring LAAs to some degree, with concomitant enlargement of LAAs. After these procedures, the values of exponent D were calculated.

Statistical Analyses

Statistical analyses were performed with JMP 7 software (SAS Institute, Cary, NC). Data are expressed as medians (25th, 75th percentile) unless otherwise indicated. Patients were divided into those with exacerbations and those without exacerbations, and differences between groups were evaluated with the Mann-Whitney *U* test. Data within groups were analyzed with the Wilcoxon signed-rank test. Relationships among data were assessed by the Spearman rank correlation test. To investigate the relative contribution of exacerbations to emphysema progression after adjustment for changes in CT-derived lung volume and baseline CT parameters of emphysema, multivariate regression analysis was performed. A P value less than 0.05 was considered significant.

RESULTS

Patient Characteristics

As shown in Figure 1, a baseline CT scan was performed on 101 patients who had already participated in our prospective observational study investigating COPD exacerbations (21–23). Of these patients, 17 were excluded because of abnormal chest shadows not associated with emphysematous changes obtained in CT images at entry. Over the next 2 years, 24 patients were excluded for the following reasons: withdrawal of consent, appearance of a new shadow on chest images, serious condition, death, or loss to follow-up. The final study population comprised 60 patients (Table 1). During the observation period, 26 patients experienced exacerbations requiring treatment with antibiotics and/or systemic corticosteroid at least once, and 34 patients experienced no exacerbations. Details of exacerbations are provided in Table E1. There were no significant differences in baseline clinical parameters, pulmonary function, or CT parameters between groups (Table 2). In addition, baseline pharmacological treatments and additional treatments were not significantly different between patients with and without exacerbations (Table E2).

Impact of Exacerbations on Lung Function and CT Parameters

We compared changes in lung function and CT parameters between patients with and without exacerbations (Table 3). There were significant annual decreases in FEV_1, $\%FEV_1$ (FEV_1 expressed as a percentage of the expected value), and ratio of diffusing capacity to alveolar ventilation (D_{LCO}/V_A) in both groups, but the degrees of decline were not significantly

TABLE 1. BASELINE CHARACTERISTICS OF STUDY PATIENTS

Characteristic	Value
Age, yr: median (25th, 75th percentile)	73.0 (68.3, 77.8)
Sex, male:female	56:4
Height, m: median (25th, 75th percentile)	1.62 (1.57, 1.68)
Weight, kg: median (25th, 75th percentile)	56.0 (49.0, 60.8)
Body mass index: median (25th, 75th percentile)	20.8 (19.5, 22.7)
Smoking status, current:former	8:52
Smoking history, pack-years: median (25th, 75th percentile)	55.0 (43.0, 84.0)
FEV_1, L: median (25th, 75th percentile)	1.27 (0.94, 1.67)
$\%FEV_1$, median (25th, 75th percentile)	50.6 (38.2, 61.1)
D_{LCO}/V_A, ml/min/mm Hg/L: median (25th, 75th percentile)	2.67 (1.90, 3.25)

Definition of abbreviations: $\%FEV_1$, FEV_1 as a percentage of the predicted value; D_{LCO}/V_A, ratio of diffusing capacity to alveolar ventilation.
n = 60 study patients.

different between the two groups. On the other hand, significant annual increases in LAA% and decreases in D were detected only in patients with exacerbations. Furthermore, changes in LAA% and D were significantly greater in patients with exacerbations than in those without (Figure 2). Increases in LAA% significantly correlated with decreases in D both in patients with exacerbations ($r = -0.50$, $P = 0.009$) and those without ($r = -0.52$, $P = 0.002$) (Figure 3). There were no significant changes in CT-derived lung volume within patients. The degrees of changes were not significantly different between the two groups (Table 2). Baseline LAA% and D significantly correlated with FEV_1, $\%FEV_1$, and D_{LCO}/V_A, whereas changes in LAA% or D did not correlate with changes in FEV_1, $\%FEV_1$, or D_{LCO}/V_A (Table E3). In stepwise multivariate regression analysis, exacerbations contributed to changes in LAA% ($R^2 = 0.41$, $P < 0.0001$) or D ($R^2 = 0.48$, $P < 0.0001$) independent of changes in lung volume and baseline CT parameters of emphysema (Table 4).

Model Simulations Using Baseline CT Images

According to our previous findings (4), we supposed that when LAA% is increased, D would decrease only if exacerbations disrupted the alveolar wall and caused the coalescence of preexisting LAAs. To test this hypothesis, we established a novel simulation model using eight baseline representative CT images. As mentioned in METHODS, model A does not allow the coalescence of LAAs, representing a case in which exacerbations lead to simple enlargement of preexisting LAAs. On the other hand, models B15 and B30 allow coalescence by the destruction of lung parenchyma between LAAs. As shown in Figure 4, model A did not lead to a decrease in D when increases in LAA% were 1, 3, and 5%. However, both model B15 and model B30 resulted in an increase in LAA% and a decrease in D. The changes in D observed in model B15 were more like the actual values seen in patients with a history of exacerbations than those in model B30.

DISCUSSION

Our study demonstrated that annual changes in CT parameters of emphysema are greater in patients with exacerbations of COPD than in those without exacerbations, and that an increase in LAA% and decrease in D reflects not only the enlargement of preexisting LAAs but also the coalescence of adjoining LAAs.

To our knowledge, this is the first longitudinal study to demonstrate the relationship between exacerbations and emphysema progression in patients with COPD. Emphysematous

TABLE 2. COMPARISON BETWEEN PATIENTS WITH AND WITHOUT EXACERBATIONS OF CHRONIC OBSTRUCTIVE PULMONARY DISEASE

Parameter	Exacerbation (–)	Exacerbation (+)	*P* Value
Subjects, n	34	26	
Exacerbations, n/yr	0	0.54 (0.49, 1.00)	
Baseline characteristics			
Age, yr	72.0 (66.0, 79.0)	73.0 (69.8, 75.5)	0.80
Sex, male:female	32:2	23:2	1.00
Body mass index	21.2 (19.6, 23.7)	20.3 (18.7, 21.9)	0.19
Smoking status, current:former	4:30	4:22	0.72
Smoking history, pack-years	52.6 (43.3, 78)	57.0 (42.5, 84.9)	0.68
FEV_1, L	1.38 (0.88, 1.67)	1.18 (0.95, 1.73)	0.58
$\%FEV_1$	50.4 (39.2, 62.9)	51.4 (37.6, 58.4)	0.77
GOLD classification, n (%)			
Stage I	1 (2.9)	1 (3.8)	
Stage II	17 (50.0)	14 (53.8)	
Stage III	14 (41.2)	8 (30.8)	
Stage IV	2 (5.9)	3 (11.5)	
D_{LCO}/V_A, ml/min/mm Hg/L	2.68 (1.88, 3.27)	2.41 (1.95, 3.24)	0.85
LAA% (−910), %	55.2 (49.2, 62.3)	59.0 (50.8, 63.0)	0.67
LAA% (−930), %	47.2 (41.4, 54.3)	50.5 (42.0, 55.5)	0.67
LAA% (−960), %	33.8 (29.3, 41.1)	36.9 (28.5, 42.3)	0.54
D	1.45 (1.16, 1.78)	1.29 (1.12, 1.69)	0.40
CT-derived total lung volume, L	5.52 (4.58, 6.03)	5.27 (4.57, 6.04)	0.87

Definition of abbreviations: $\%FEV_1$, FEV_1 as a percentage of the predicted value; CT = computed tomography; D_{LCO}/V_A, ratio of diffusing capacity to alveolar ventilation; GOLD = Global Initiative for Chronic Obstructive Lung Disease; LAA%, percentage of low-attenuation area.
Data are expressed as medians (25th, 75th percentile) unless otherwise indicated.

changes have been assessed mainly by CT in cross-sectional studies (3, 4, 10, 11, 24, 25). Few longitudinal studies have been performed in patients with COPD without α_1-antitrypsin deficiency.

Exacerbations are important events in patients with COPD because they contribute to the further decline of lung function (5), impaired health-related quality of life (6, 7), socioeconomic burden (9), and poor prognosis (8). Given that airway inflammation, oxidative stress, and proteolysis are involved in the pathogenesis of COPD (1) and are enhanced in exacerbations (1, 27–30), we assumed that exacerbations would affect lung pathological changes such as emphysema. However, their impact on emphysema progression has not been investigated. In addition, we previously demonstrated that emphysematous changes assessed by CT correlated with COPD mortality, independent of lung function (16). Therefore, this study gives us important insight into the mechanism of emphysema progression and the management of patients with COPD.

We analyzed not only LAA% but also D to explore the mechanism of emphysema progression. The cumulative size distribution of the LAA clusters has been shown to follow a power law characterized by exponent D (4, 31–33). The values of D can be obtained by linear regression and calculated as the slope of the straight line in the log–log plot. The goodness-of-fit was assessed by the correlation coefficients (r). We determined that the values of r in all images were greater than 0.941, and that the mean ± SD values of r in patients with and without exacerbations were 0.988 ± 0.009 and 0.987 ± 0.009, respectively. These values are consistent with those reported in our previous study (4). The exponent D reflects the fractal dimension of terminal airspace geometry (4). Analyzing the fractal property has been shown to be useful for detecting early stages of COPD, predicting survival (33) or exercise capacity after lung volume reduction surgery in patients with COPD (32), and discriminating between hyperinflation and emphysema in patients with asthma (31). Other investigators have reported that microscopically measured mean perimeters of alveoli and alveolar ducts and mean interwall distances are correlated with

TABLE 3. ANNUAL CHANGE IN LUNG FUNCTION AND COMPUTED TOMOGRAPHY PARAMETERS: INTRA- AND INTERGROUP COMPARISONS BETWEEN PATIENTS WITH AND WITHOUT EXACERBATIONS OF CHRONIC OBSTRUCTIVE PULMONARY DISEASE

	Exacerbation (–)		Exacerbation (+)		
Parameter	Value	*P* Value (within Group)	Value	*P* Value (within Group)	*P* Value (between Groups)
FEV_1, ml	−43.7 (−90.1, −3.38)	0.002	−73.9 (−91.9, −4.7)	0.0002	0.46
$\%FEV_1$	−1.10 (−3.02, 0.67)	0.05	−2.05 (−3.07, 0.29)	0.01	0.40
D_{LCO}/V_A, ml/min/mm Hg/L	−0.50 (−1.25, −0.08)	0.0008	−0.53 (−1.39, 0.03)	0.002	0.97
LAA% (−910), %	0.16 (−0.38, 0.98)	0.18	1.63 (0.80, 2.42)	<0.0001	0.0002
LAA% (−930), %	0.24 (−0.46, 0.66)	0.27	1.92 (0.92, 2.70)	<0.0001	<0.0001
LAA% (−960), %	0.13 (−0.34, 0.68)	0.21	2.10 (1.09, 2.82)	<0.0001	<0.0001
D	−0.015 (−0.027, 0.015)	0.09	−0.059 (−0.010, −0.041)	<0.0001	<0.0001
CT-derived total lung volume, ml	52.0 (−88.8, 273.3)	0.11	−45.5 (−255.0, 223.3)	0.52	0.14

Definition of abbreviations: $\%FEV_1$, FEV_1 as a percentage of the predicted value; CT = computed tomography; D_{LCO}/V_A, ratio of diffusing capacity to alveolar ventilation; LAA%, percentage of low-attenuation area.

Data are expressed as medians (25th, 75th percentile).

LAA% but not D (14). These reports suggest that LAA% and D are complementary tools in the assessment of emphysema. Therefore, the combination of analyzing fractal properties by D and quantifying emphysematous change by LAA% could give us greater insights than measuring only LAA%.

In this study, increases in LAA% and decreases in D were greater in patients with exacerbations than in those without exacerbations. The relationship of exacerbations to changes in these CT parameters of emphysema persisted after adjusting for baseline CT parameters. Furthermore, changes in LAA% showed a significant inverse correlation with changes in D. In our previous report (4), patients with COPD had a smaller D than healthy subjects. We interpreted these results by simulations using a two-dimensional elastic spring network model, and demonstrated that a break of the alveolar wall and coalescence of preexisting LAA clusters could reduce values of D but leave LAA% unchanged. We thus supposed that the destruction of alveolar walls and the coalescence of neighboring LAAs occur more frequently in patients with exacerbations than in those without, and that these structural changes are reflected by an increase in LAA% and decrease in D.

Given that our previous study was cross-sectional and that its simulation included an unchanging LAA%, we established a new simulation model in the present study to assess our hypothesis. Consequently, our observed result could not be reproduced by model A, which does not allow the coalescence of neighboring LAAs due to alveolar wall destruction. We therefore performed simulations using models B15 and B30, in which 15 or 30%, respectively, of selected pixels caused the coalescence of preexisting LAAs, while the remaining selected pixels only caused simple enlargement.

As shown in Figure 4, model B15 elegantly reproduced a reduction of D observed in patients with a history of exacerbations. This suggests that both destruction of the alveolar wall separating adjoining LAAs and enlargement of preexisting LAAs occur in exacerbations. We assume that preexisting LAAs could be more pathogenic than normal lung areas, and alveolar walls separating adjoining LAAs might be more vulnerable than those separating LAAs and normal lung areas. Enhanced airway inflammation, oxidative stress, and protease induction during exacerbation might contribute to this phenomenon.

We investigated the impact of exacerbations requiring systemic steroid and/or antibiotic treatment and then demonstrated that exacerbations are associated with emphysema progression. This suggests that the current dose and timing of such treatments might not be sufficient to prevent further emphysema progression in patients with COPD exacerbations. Although systemic steroid and antibiotics have been shown to be effective for relieving clinical symptoms and lung function (34–37), their

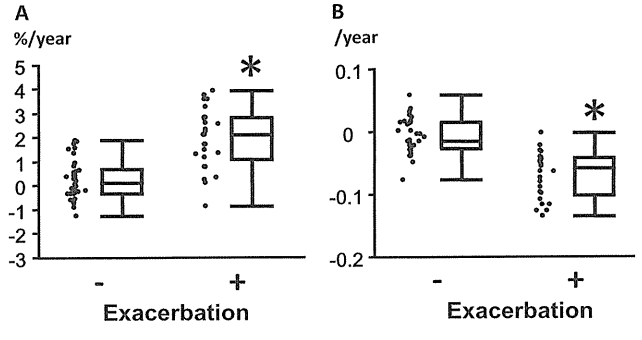

Figure 2. Change in (*A*) LAA% and (*B*) D in patients with and without a history of exacerbations (n = 26 and 34, respectively). *$P < 0.0001$ compared with patients without exacerbations. The *horizontal line* is the median value, the *box* is the interquartile range, and the *whiskers* indicate the range, excluding outlying and extreme values (i.e., points with values ⩾ 1.5 box lengths from the upper or lower limits of the *box*). LAA% = percentage of the lung field occupied by low-attenuation areas.

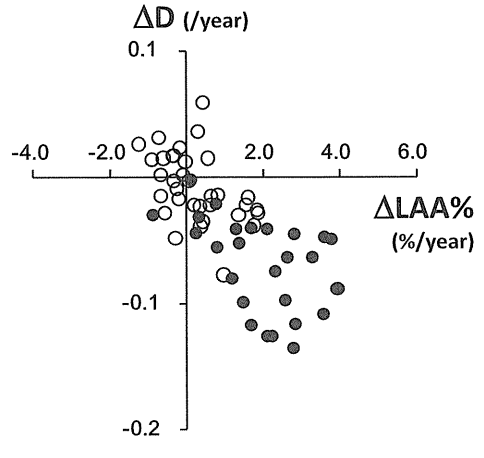

Figure 3. Relationship between changes in LAA% and D both in patients with and without a history of exacerbations. *Solid circles* and *open circles* show the change in patients with and without exacerbations, respectively. A significant correlation between an increase in LAA% and a decrease in D was found in each group ($r = -0.50$, $P = 0.009$ and $r = -0.52$, $P = 0.002$). LAA% = percentage of the lung field occupied by low-attenuation areas.